Development of textural differentiation in soils: a quantitative analysis

Thesis submitted in accordance with the requirements of the University of Adelaide for an Honours Degree in Environmental Geoscience

Matthew Bald

November 2012

THE UNIVERSITY
of ADELAIDE

TITLE

Development of textural differentiation in soils: a quantitative analysis

RUNNING TITLE

Textural differentiation in soils

ABSTRACT

A soil profile exhibiting strong textural differentiation between surface and subsurface horizons at Keyneton, South Australia, was sampled for quantitative and qualitative analyses of the processes responsible for development. From constant resistant mineral ratios throughout the profile it was concluded that the soil had formed from uniform parent material, suggesting that pedological processes had heavily influenced formation. Particle size distribution, clay mineralogy determined by XRD, and microstructural features indicated that clay accumulation in the subsurface was accompanied by a greater intensity of weathering in the surface horizons. The presence of void argillans in the B horizon provided strong evidence for the translocation of clay. Mass balance calculations showed significant volumetric expansion and mass gain throughout the entire profile, but greatest in the B horizons. Al, Fe, Na and Si were all gained in large quantities. The results indicate that clay translocation by illuviation is a dominant process in the development of textural differentiation, with some clay likely to have formed *in situ*.

KEYWORDS

TABLE OF CONTENTS

LIST OF FIGURES AND TABLES

INTRODUCTION

Multiple hypotheses have been proposed to explain the formation and development of strong texture contrast between surface and subsurface horizons in soil profiles; a feature that is common to many soils of Australia, as well as other climate-and-lithology specific localities around the world. Possible mechanisms for the development of texture contrast include the inheritance of textural stratification from parent material, translocation of clay, differential weathering of soil horizons, and bioturbation. Despite numerous studies, the processes resulting in this common soil feature remain subject to debate, with all of above mechanisms appearing plausible. Given that texture contrast has a profound impact on both hydrological and biological systems, a better understanding of the process of formation would be of benefit to landscape management strategies, soil classification systems, and engineering endeavours.

Previous studies of Australian soils exhibiting texture contrast by Oertel (1974) and Bishop *et al.* (1980) concluded that separate sedimentary origins of the parent material were responsible for the observed textural differentiation. These findings were challenged by Chittleborough & Oades (1980a) and Chittleborough *et al.* (1984b, 1984c) who concluded from physical and chemical data that soil horizons of contrasting texture were in fact derived from uniform parent material. The argument for inheritance of textural stratification from parent material was maintained after Krull *et al.* (2006) completed comprehensive chemical and mineralogical analyses of organic matter from three South Australian soils, concluding that two distinct depositional events were responsible for texture contrast. Controversy abounds.

Other common hypotheses for the formation and development of texture contrast soils propose pedogenic processes, such as the formation of clay in position by means of differential weathering, as primary causes. Indices of chemical weathering developed by Beavers *et al.* (1963) were applied to a texture contast soil profile by Chittleborough & Oades (1979, 1980b) who determined that there was no significant change in the degree of weathering with depth, concluding that the translocation of clay by illuviation was instead responsible for the textural differentiation and high clay content observed in the subsurface.

The aforementioned process of clay illuviation has become widely accepted as a key process in the development of many texture contrast soils; however, Phillips (2001) states that soils must be considered subject to both historical and spatial contingency, emphasising that it is impractical to develop a generalisation for the formation of a soil feature such as texture contrast. Chittleborough (1992) acknowledges that no single explanation is likely to account for the development of textural differentiation, a view that is embodied by the 'multiple causality' model proposed by Phillips (2004) in which texture contrast is considered to result from a combination of pedological processes.

Proposing 'multiple causality' as the mode of development for all texture contrast soils is in itself a generalisation and, given that previous studies have been largely qualitative, it is likely that the quantification of processes involved in pedogenesis would provide a more robust explanation. The method of mass balance reconstruction developed by Brimhall *et al.* (1987, 1991, 1992) and Chadwick *et al.* (1990) enables losses and gains of chemical constituents from soil profiles to be quantified, along with

changes in volume and mass. The application of mass balance analyses, in conjunction with mineralogical and micro-structural data, provides a pathway for comprehensive investigations into the mechanisms contributing to soil formation.

In this study the losses and gains of mass, volume, and a select group of elements are quantified in a soil profile at Keyneton, South Australia. The uniformity of the parent material, particle size distribution, microstructural features, degree of weathering, and the nature of the clay particles from the profile are also investigated to determine the processes involved in the development of textural differentiation between surface and subsurface horizons.

GEOLOGICAL SETTING/BACKGROUND

Study site description

The Keyneton soil profile sampled for this study is located 65 km northeast of Adelaide on the eastern flank of the Mount Lofty Ranges, South Australia (Figure 1). The site can be found at latitude 34° 32' 5" S and longitude 139° 8' 30" E upon the Kanmantoo Group sedimentary rocks of the Adelaide Geosyncline (Jago *et al.* 2003). A geological survey of a study area 5 km north of Keyneton by McMaster (1992) identified the presence of rocks from both the Backstairs Passage Formation and the Campana Creek Member of the Carrickalinga Head Formation. The Backstairs Passage Formation conformably overlies the Campana Creek Member and both units are largely composed of medium-grained arkosic sandstone; however, the sandstones of the Backstairs Passage Formation have been noted to be richer in quartz (Gatehouse *et al.* 1990; Jago

et al. 2003). These sandstone units are considered to be the geological precursors to the soil and weathering profiles observed at Keyneton.

Figure 1: Locality map of the study site, Keyneton, South Australia.

A soil survey by Fitzpatrick *et al*. (1990) found that the predominant soil types of the local area displayed strong texture contrast between surface and subsurface horizons. Quartz fragments were abundant and the identification of argillic B horizons led to the classification of these soils as Alfisols (Fitzpatrick *et al*. 1990; Soil Survey Staff 1999, 2010). The particular Alfisol sampled for this investigation contains a very high percentage of ironstone gravel and was further classified as a Natric Palexeralf (Fitzpatrick *et al*., 1990; Soil Survey Staff, 1999, 2010).

The sampling site lies at an altitude of 400 m and experiences a Mediterranean climate with a mean annual rainfall of 535 mm, majority of which occurs from May to September (Bureau of Meteorology, 2011). Due to the climatic conditions, the Keyneton profile has formed in a strong seasonal wetting and drying moisture regime. Present vegetation at the study site comprises undisturbed native plants and grasses; however, much of the surrounding land has been cleared for agricultural purposes.

Background

TEXTURE CONTRAST IN SOIL CLASSIFICATION SYSTEMS

Strong texture contrast between surface and subsurface horizons is an important diagnostic property incorporated into the hierarchy of many soil classification systems (Stace *et al.* 1968; Isbell 1996; Soil Survey Staff 1999, 2010). Isbell (1996) defined textural differentiation as a clear or abrupt boundary, usually between A and B horizons, accompanied by an increase in clay. This is similar, but not equivalent, to the definition of the term 'duplex' which describes soils where the B horizon is at least one and a half texture groups finer than the A horizon with a clear boundary (Northcote 1979). In relation to texture contrast soils, national and international soil classification systems also use the term 'argillic horizon' to describe the subsurface accumulation of clay either *in situ* or via translocation.

THE GEOLOGICAL HYPOTHESES

A common explanation for the formation and development of texture contrast is that the differentiation is directly inherited from stratified parent material. Resistant minerals

such as zircon, rutile and xenotime are crucial to investigations assessing the uniformity of a parent material as they are assumed to remain relatively inert and immobile during weathering and pedogenesis. A study of elemental concentrations and particle size distribution from a South Australian texture contrast soil by Oertel (1974) concluded that the A and B horizons of the profile had originated from separate sedimentary deposits. A later study by Chittleborough & Oades (1980a) investigated the same soil profile, using distributions and ratios of resistant minerals from a range of particle size fractions to determine that the soil had in fact formed from uniform parent material. The contrasting results from studies of near-identical profiles emphasise the need for a variety of criteria to be considered in studies assessing parent material uniformity.

Scanning electron microscopy (SEM) and energy dispersive x-ray analysis (EDAX) were used by Anda *et al*. (2009) in assessing parent material uniformity of three South Australian texture contrast soils, all of which were derived from different parent materials. These techniques allowed the determination of which resistant minerals could be considered reliable for use in assessing parent material uniformity. Results indicated that two of the three soil profiles had inherited textural contrast from lithological discontinuities in the parent material, whilst the remaining profile showed little variation in resistant mineral concentrations with depth (Anda *et al*. 2009). This suggested that it had formed from uniform parent material with the observed textural differentiation therefore being a result of pedological processes.

In addition to *in situ* inheritance of texture contrast from stratified parent material, the processes of erosion and deposition provide another geological pathway for the

formation of texture contrast soils. A study of textural differentiation in soils on hillslopes in New South Wales by Bishop (1980) concluded that lateral downslope deposition and accumulation of coarse grained material was responsible. Bishop (1980) suggested that this explanation may have a very wide application in describing the formation of texture contrast soils. Given that these soils are common in relatively flat landscapes, this suggestion seems unlikely to be broadly applicable; however, other workers have also proposed multiple depositional events as the main factor in generating texture contrast.

Krull et al. (2006) analysed the organic geochemistry of three South Australian texture contrast soils, noting that there were considerable differences between the coarse grained A horizons and the clay rich B horizons. Coupled with optically stimulated luminescence dating of quartz grains to determine burial ages, it was inferred from the geochemical data that the sandy surface horizons were largely aeolian in origin and deposited much more recently than the clay-rich subsurface material. Geological controls without doubt play a large role in the formation of soil profiles; however, many studies proposing a geological origin of features such as texture contrast only follow a single line of enquiry, failing to investigate the role or extent of pedological processes.

THE PEDOLOGICAL HYPOTHESES

When considering the formation and development of texture contrast soils resulting from pedological processes, a prevalent explanation is the translocation of clay. This process involves the vertical transport of clay down a soil profile with percolating water, resulting in coarse grained surface horizons and clay-rich subsurface horizons. Void argillans, or clay skins, are considered key physical evidence for the accumulation

of clay via translocation (Soil Survey Staff 1999, 2010); however, Nettleton *et al*. (1969) demonstrated that shrinking and swelling processes associated with seasonal wetting and drying of soils were sufficient to destroy existing argillans, indicating that their absence cannot rule out clay translocation as a mechanism responsible for textural differentiation. Studies by Chittleborough & Oades (1980a, 1980b) and Chittleborough *et al*. (1984b, 1984c) concluded that vertical translocation of clay was the primary process responsible for texture contrast, but also acknowledged that the *in situ* formation of clay by differential weathering had contributed.

For a texture contrast soil to form via *in situ* clay formation, there must generally be differential weathering between the surface and subsurface soil horizons (Chittleborough, 1992). In most occurrences of texture contrast, coarse material overlies fine material; therefore, weathering would need to be more intense in the subsurface horizons. An alternative explanation is that the extent of weathering is similar throughout a profile, with surface clay lost from the profile by lateral transport. For profiles deemed to have originated from uniform parent material, numerous indices have been developed to assess the degree of weathering. The chemical index of alteration (CIA) proposed by Nesbitt & Young (1982) and the chemical index of weathering (CIW) by Harnois (1988) are two commonly used indices for the quantification of weathering; however, they assume immobility of aluminium. Chittleborough (1991) identified limitations of the indices given that aluminium is commonly incorporated into clay minerals which can often be mobile in weathering profiles. Most pedological studies utilising weathering indices have concluded that

weathering is either relatively uniform throughout the profile or more intense in surface horizons.

In addition to translocation of clay and *in situ* weathering, bioturbation has also been considered as a pedological process with the potential to result in textural differentiation. Burrowing animals, as well as root systems, have been shown to have a significant influence on the mobility of both organic and inorganic material within soil profiles (Brimhall *et al*. 1992). Nooren *et al*. (1995) determined that earthworms had contributed to the development of coarse grained surface horizons, with the erosion and translocation of worm casts resulting in a clay-rich subsurface. The work of Johnson *et al*. (1990) noted that depth of bioturbation, in conjunction with moisture regimes, are important factors in the formation of texture contrast soils. More so than other pedogenic processes, bioturbation is unique to specific locations; therefore, it is unlikely to be a widely applicable explanation for the genesis of texture contrast in soil profiles.

THE MULTIPLE CAUSALITY HYPOTHESIS

Much of the previous work investigating the formation and development of texture contrast soils has produced explanations that are only applicable to specific soil profiles or landscapes. Significant debate and controversy surrounds the search for a general explanation that is able to account for all texture contrast soils. Phillips (2001) noted that soils are subject to historical and spatial contingency and emphasised that generalisations for the occurrence of widespread morphological features in soil profiles are often impractical. This idea supports the suggestion of Chittleborough (1992) that the extensive diversity and distribution of texture contrast soils makes a single explanation for their formation unlikely. Phillips (2004) proposed a model of 'multiple

causality' in which the formation and development of texture contrast is attributed to any combination of pedological processes known to operate globally. Although useful, the 'multiple causality' model is very broad and may be better constrained with the use of quantitative techniques.

MASS BALANCE RECONSTRUCTION

Advanced methods for the quantification of pedological processes were developed by Brimhall *et al*. (1987, 1991, 1992) and Chadwick *et al*. (1990) based on the principle of conservation of mass. The methods allow the volume and mass changes that occur during soil formation to be quantified along with the loss or gain of chemical constituents. Mass balance reconstructions and techniques have been applied in many studies (Jersak *et* al. 1995; Driese *et al*. 2000; Klaminder & Yoo 2008; Heckman & Rasmussen 2011); however, the potential of the techniques has yet to be focussed on the development of textural differentiation in soil profiles. Herein, an attempt to remedy this deficiency is made.

METHODS

Field sampling

The Keyneton soil profile sampled for this study was located 65 km northeast of

Adelaide at latitude 34° 32' 5" S and longitude 139° 8' 30" E (Figure 1), where an

excavator was used to dig a pit to 1.6 m depth. The soil profile was described in the

field and representative bulk samples of each horizon were taken from the face of the

excavation, along with intact clods.

Laboratory methods

The bulk density of each horizon was determined by the intact clod method outlined by

Grossman & Reinsch (2002) and corrected for gravel content by incorporating the

method of Carter (1993) (see Appendix G for detailed descriptions). Particle size

analysis of the profile was carried out using the hydrometer method described by Gee &

Or (2002), in addition to separation of particle size fractions by wet sieving (see

Appendix B for detailed descriptions). Subsamples of suspensions from the particle size

distribution work were analysed using x-ray diffraction (CoKα radiation) by CSIRO

Land & Water (see Appendix I for a detailed description). The bulk soil from each

horizon, in addition to subsamples from the 20-63 μm and 63-125 μm size fractions

separated during sieving analysis, were analysed for chemical composition by ICP-OES

and ICP-MS at Intertek Genalysis (see Appendix D for a detailed description).

Thin sections of intact samples were cut at Earthslides (UK), following de-watering by

acetone replacement and impregnation with casting resin. Transmitted cross-polarised

light microscopy was then carried out on the Nikon LV100 POL petrographic

microscope at Adelaide Microscopy to examine microstructural features (see Appendix C for a detailed description).

Evaluation of parent material uniformity

Ratios of minerals known to be resistant to weathering were calculated throughout the Keyneton profile from elemental concentrations. Ratios of Zr:Ti, Nd:Zr, Y:Zr, and Nb:Zr were used given the common occurrence of these elements in zircon, rutile, xenotime, and monazite. For three of the ratios, only data from the 20-125 μm size fraction was considered due to the relative abundance of resistant minerals in that particle size range. A constant elemental ratio down the soil profile is indicative of uniform parent material, while a deviation suggests possible lithologic discontinuity (Anda *et al*. 2009). Ratios such as these have been used to assess parent material uniformity in many studies, including those by Chittleborough *et al*. (1984c) and Smeck *et al*. (1994).

Determining the extent & intensity of weathering

The chemical index of alteration (CIA) proposed by Nesbitt & Young (1982), an index often used to quantify the extent of chemical weathering, was applied to the Keyneton profile. The index is calculated as follows:

$$CIA = [Al_2O_3/(Al_2O_3 + CaO + Na_2O + K_2O)]*100$$

Concentrations of the oxides are given as molar proportions with a resultant CIA value of ≤ 50 assumed to represent fresh rock and a value of ~100 taken to represent highly weathered material.

Mass balance reconstruction

Calculation of losses and gains of volume, mass, and chemical constituents were implemented, based on the methods developed by Brimhall *et al.* (1987, 1988, 1991, 1992), Chadwick *et al.* (1990), and Brewer (1976) (see Appendix H for a detailed description).

The strain ($\varepsilon_{Zr,w}$), or volume change, of each horizon was calculated using Zr as an immobile element within the profile from the following equation (Chadwick *et al.* 1990):

$$\varepsilon_{Zr,w} = [\,(\rho_p C_{Zr,p})/(\rho_w C_{Zr,w})\,] - 1$$

Where ρ_p is the bulk density of the parent material, ρ_w is the bulk density of the weathered soil horizon, $C_{Zr,p}$ is the concentration of Zr in the parent material, and $C_{Zr,w}$ is the concentration of Zr in the weathered soil horizon. Where a deviation from the bulk density of the parent material occurs, that is not accompanied by an inversely proportional change in Zr concentration, it is deemed that strain (volume change) has taken place (Chadwick *et al.* 1990). Positive strain indicates the fraction of volume gained, and negative strain indicates the fraction of volume lost.

Using the strain values, the loss or gain of a select group of elements for each horizon were calculated in the form of the transported mass fraction ($\tau_{j,w}$) (Chadwick *et al.* 1990):

$$\tau_{j,w} = [\,(\rho_w C_{j,w})/(\rho_p C_{j,p})\,] \times (\varepsilon_{Zr,w}+1) - 1$$

Where ρ_p is the bulk density of the parent material, ρ_w is the bulk density of the weathered soil horizon, $C_{j,p}$ is the concentration of the element of interest in the parent material, and $C_{j,w}$ is the concentration of the element of interest in the weathered soil horizon. Similarly to strain, the transported mass fraction has no units, and represents the fraction of an element gained or lost from a horizon.

Finally, the change in mass of the Keyneton profile during pedogenesis was calculated using a method largely derived from Brewer (1976):

$$\Delta m = m_p - m_w$$

The change in mass of a horizon (Δm) was given as the difference between the mass of the parent material (m_p) and the mass of the weathered soil horizon (m_w). The mass of the weathered soil horizon, m_w, was calculated by setting the volume of each horizon equal to $1 cm^2$ multiplied by the corresponding depth. The mass of the parent material was determined as follows:
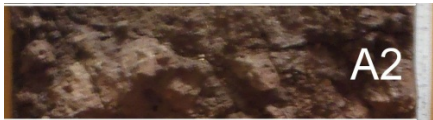
$$m_p = (C_{Zr,w}/C_{Zr,p}) \times m_w$$

Where $C_{Zr,w}$ is the concentration of Zr in the weathered soil horizon and $C_{Zr,w}$ is the concentration of Zr in the parent material.

OBSERVATIONS AND RESULTS

Soil description

Table 1: Description of the Keyneton soil profile with texture classes assigned in accordance with the Australian Soil Classification (Isbell, 1996).

Horizon	Depth (cm)	Description	Profile
A1	0 – 8	Dark brown loam with weak granular structure and abundant organic matter. Abrupt to:	
A2	8 – 18	Medium brown sandy loam with moderate granular structure. Abrupt to:	
B21	18 – 33	Brown red clay with strong angular blocky structure. Contains 10-20% ironstone & quartz gravel. Gradual to:	
B22	33 – 54	Orange brown clay with strong angular blocky structure. Contains 15-25% ironstone & quartz gravel. Gradual to:	
C	54 – 80	Light brown orange clay loam with subangular blocky structure. Contains 5-15% quartz gravel. Diffuse to:	
R	80 – 100	Light grey fine grained arkosic sandstone. Evidence of weathering including iron oxide staining on some surfaces.	-

Particle size distribution
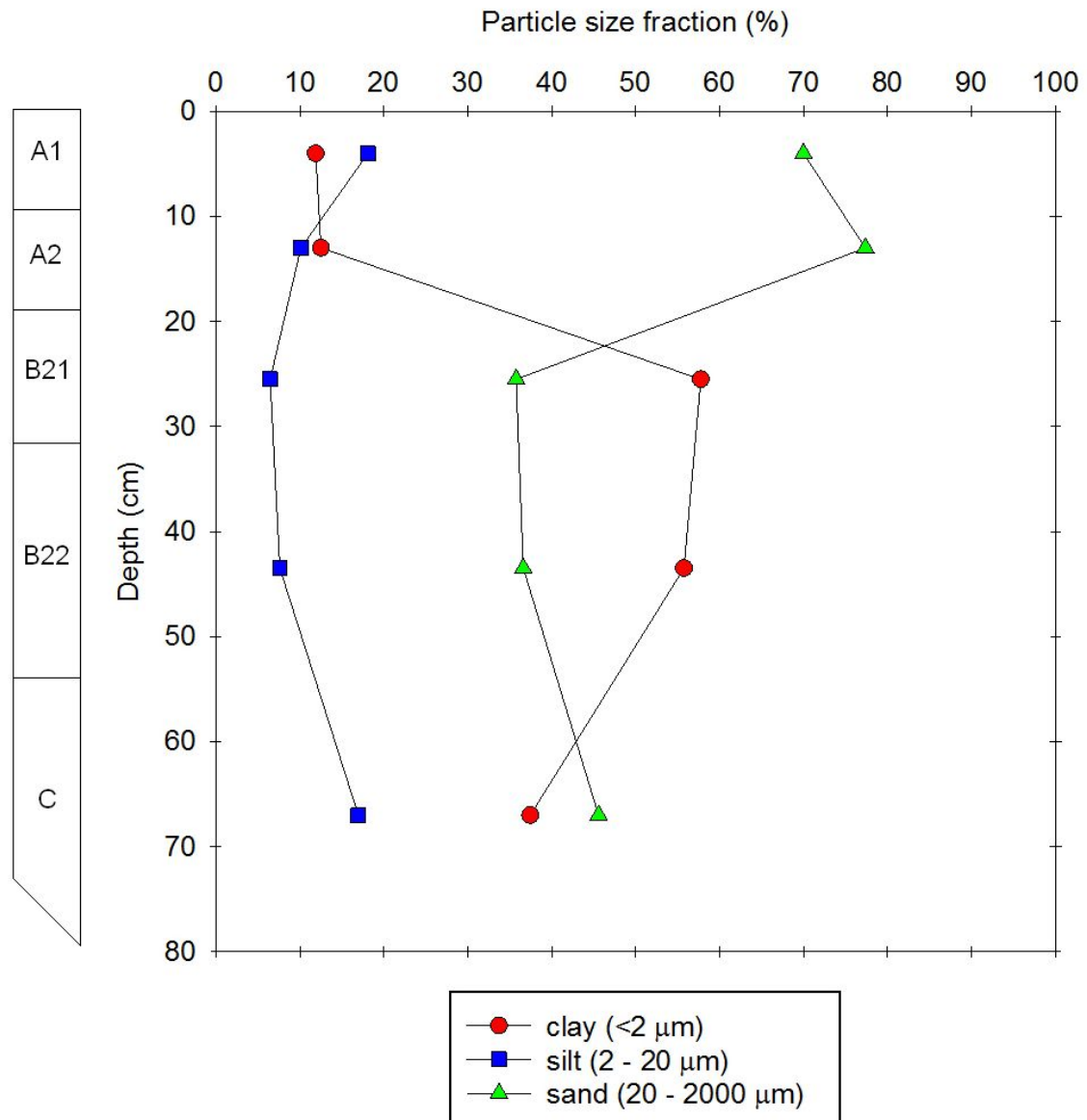
Figure 2: Particle size distribution depth plot of the fine earth fraction (≤2000 µm) from the Keyneton soil profile obtained via the hydrometer method outlined by Gee & Or (2002).
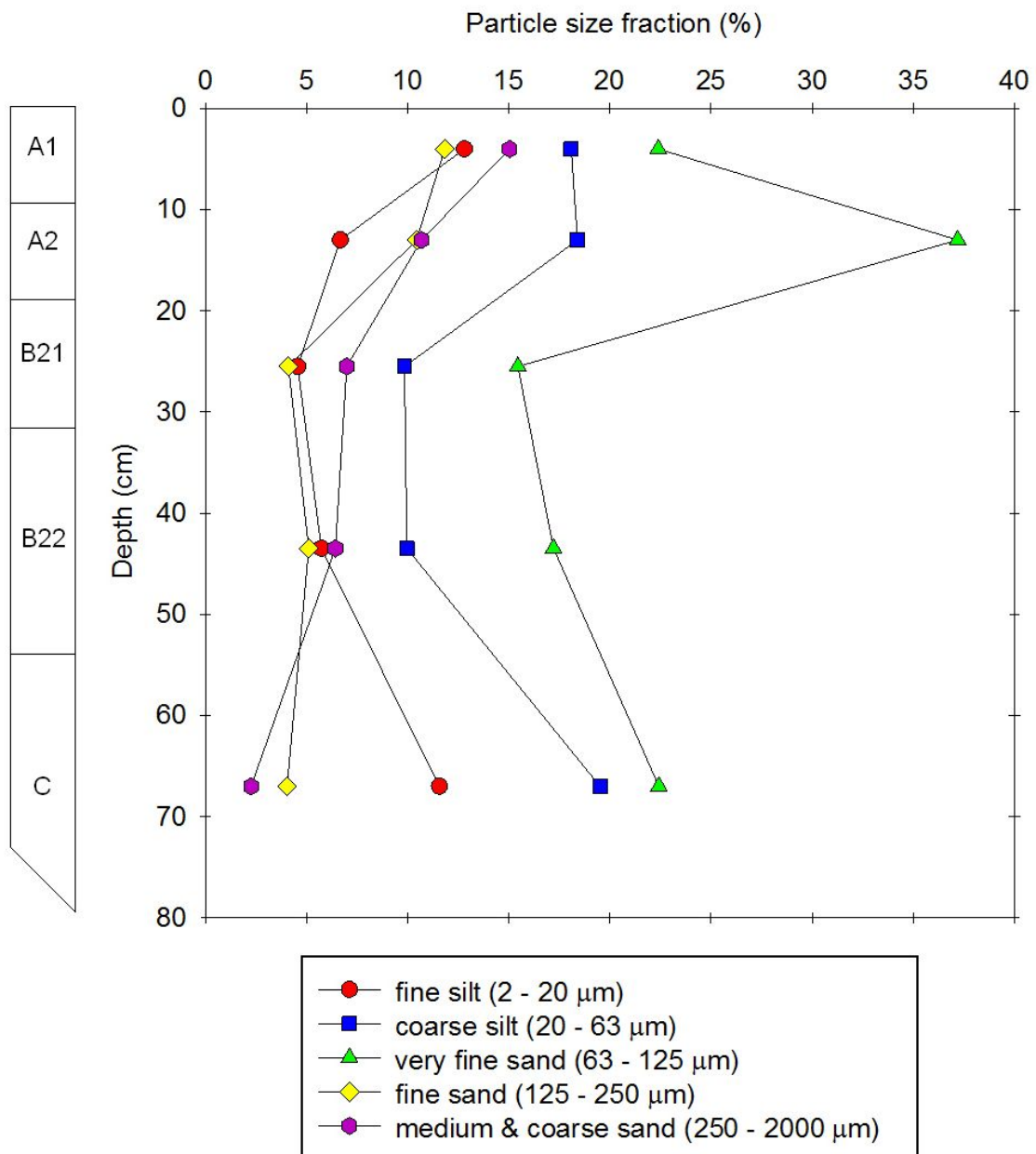
Figure 3: Particle size distribution depth plot of the sand & silt from the fine earth fraction (≤2000 μm) of the Keyneton soil profile, determined by sieving analysis.
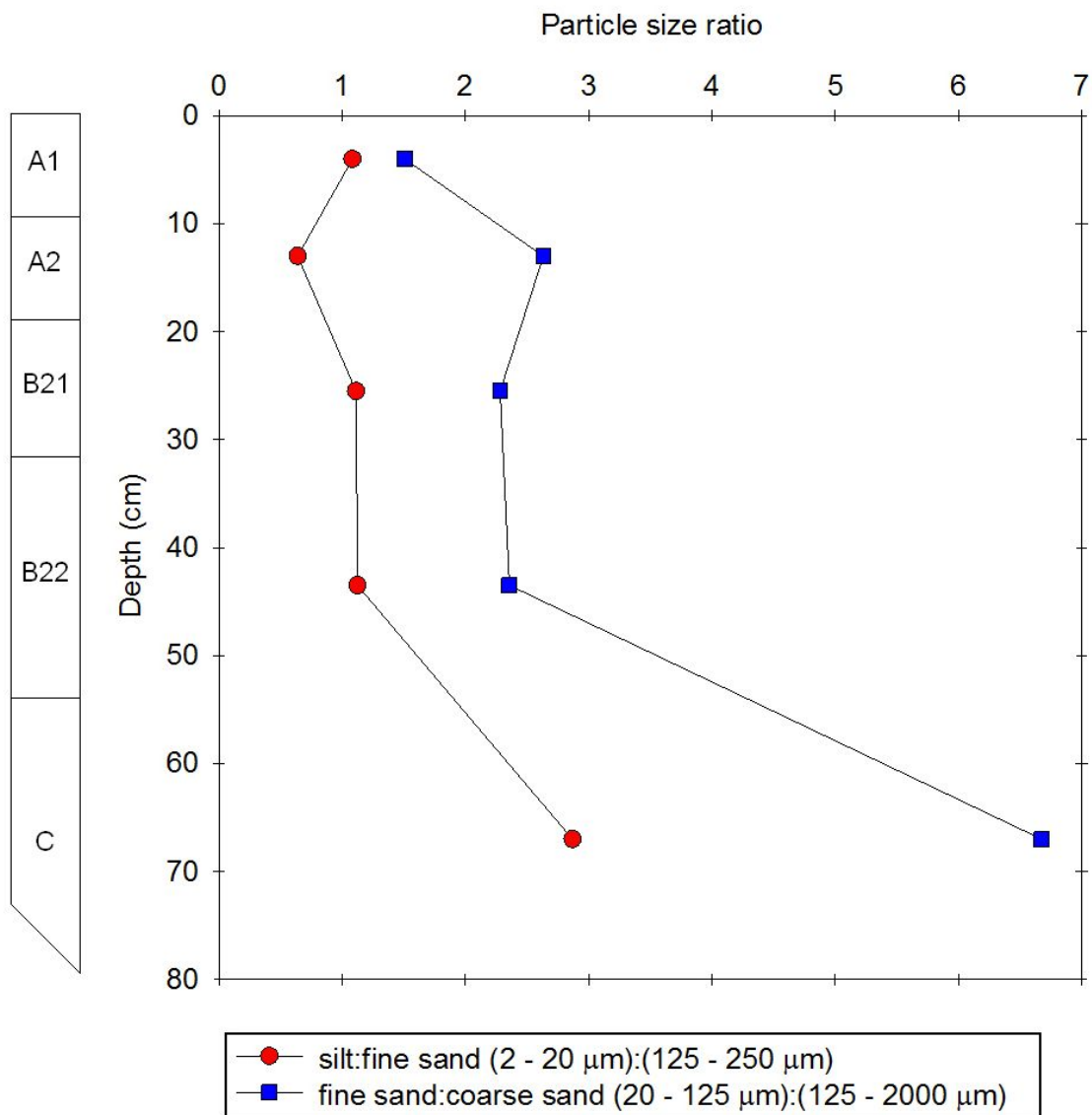
Figure 4: Depth plot of particle size fraction ratios from the Keyneton soil profile. The particle size fractions utilised in these ratios were obtained by sieving analysis.
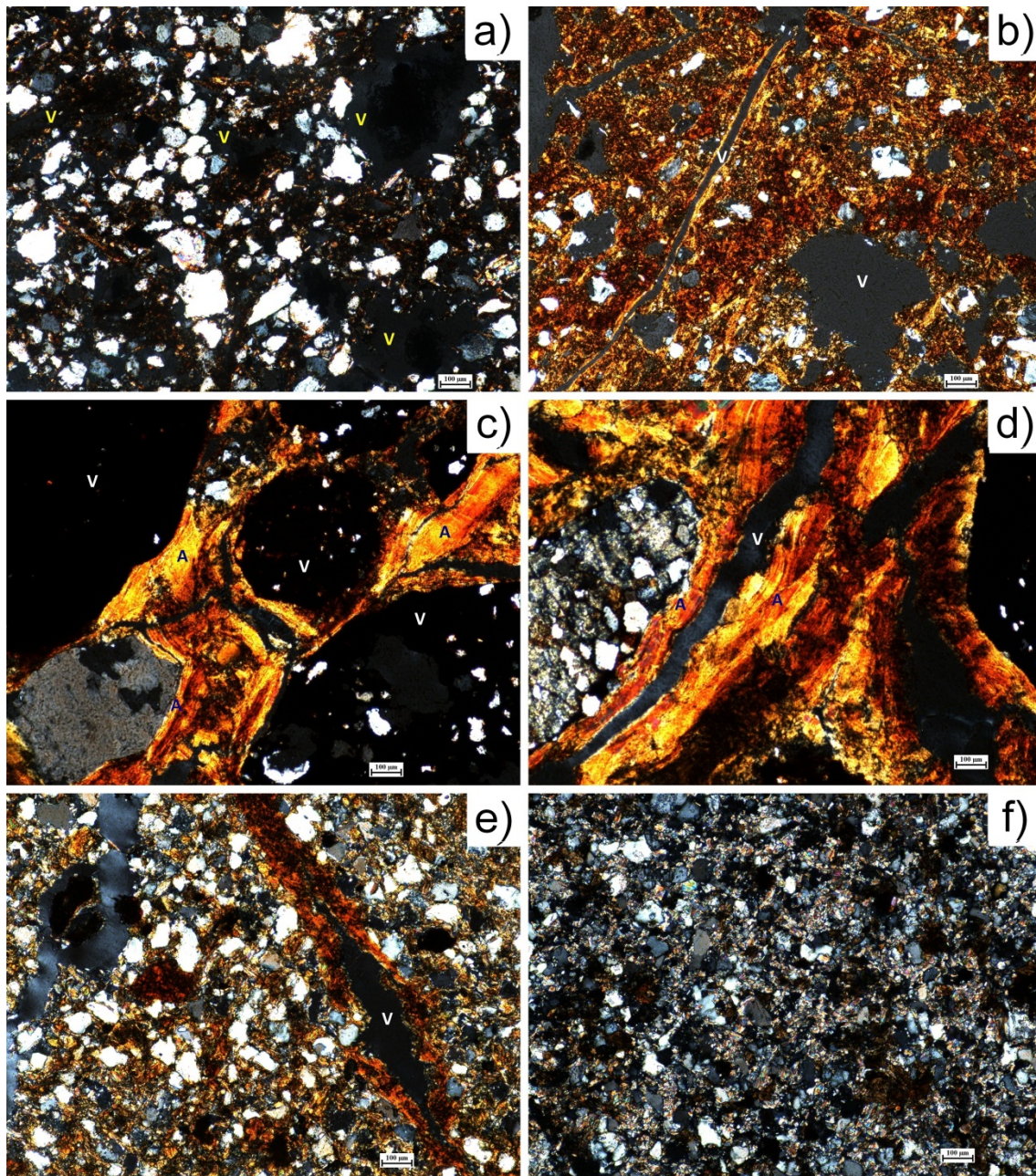
Figure 5: Transmitted cross-polarised light micrographs of the Keyneton soil profile. Horizons shown are: a) A2, b) B21, c) & d) B22, e) C, and f) R. The images are annotated with 'V' to indicate void space and 'A' to indicate argillans (clay skins).

Evaluation of parent material uniformity
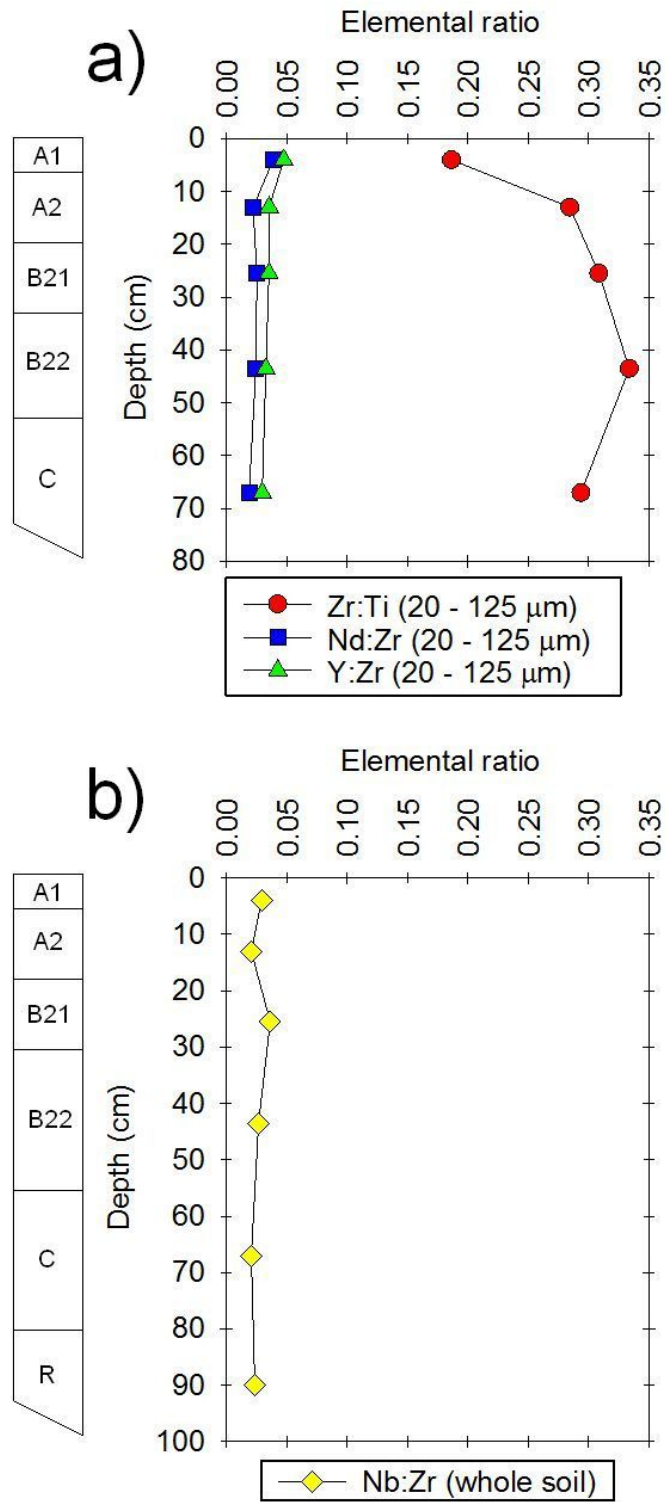
Figure 6: Depth plots of elemental ratios from the Keyneton soil profile. Ratios of a) Zr:Ti, Nd:Zr, and Y:Zr from the 20-125 μm fraction are shown in addition to b) the Nb:Zr ratio from the whole soil fraction.

Determining the extent & intensity of weathering
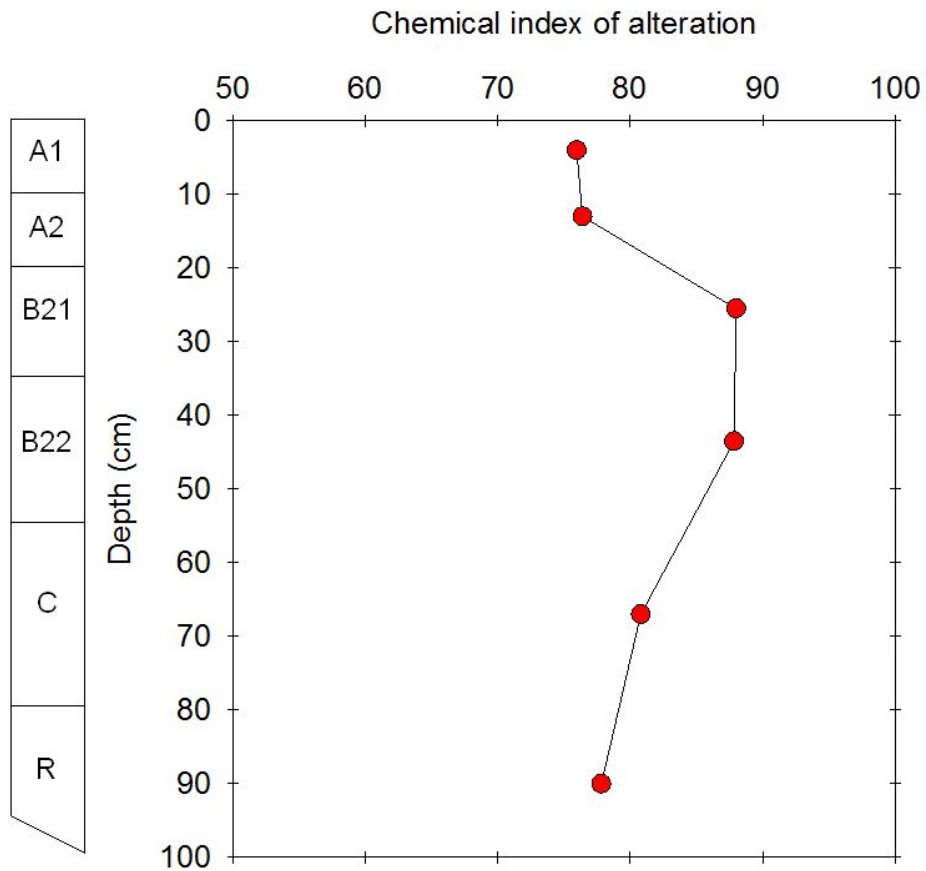
Figure 7: Depth plot of the chemical index of alteration (CIA) throughout the Keyneton soil profile. The index assumes immobility of aluminium and mobility of calcium, sodium and potassium. The resultant value has no units, but quantifies the degree of weathering. Values of ≤50 expected for fresh rock and values of approximately 100 expected for samples with the highest degree of weathering (Nesbitt & Young, 1982).
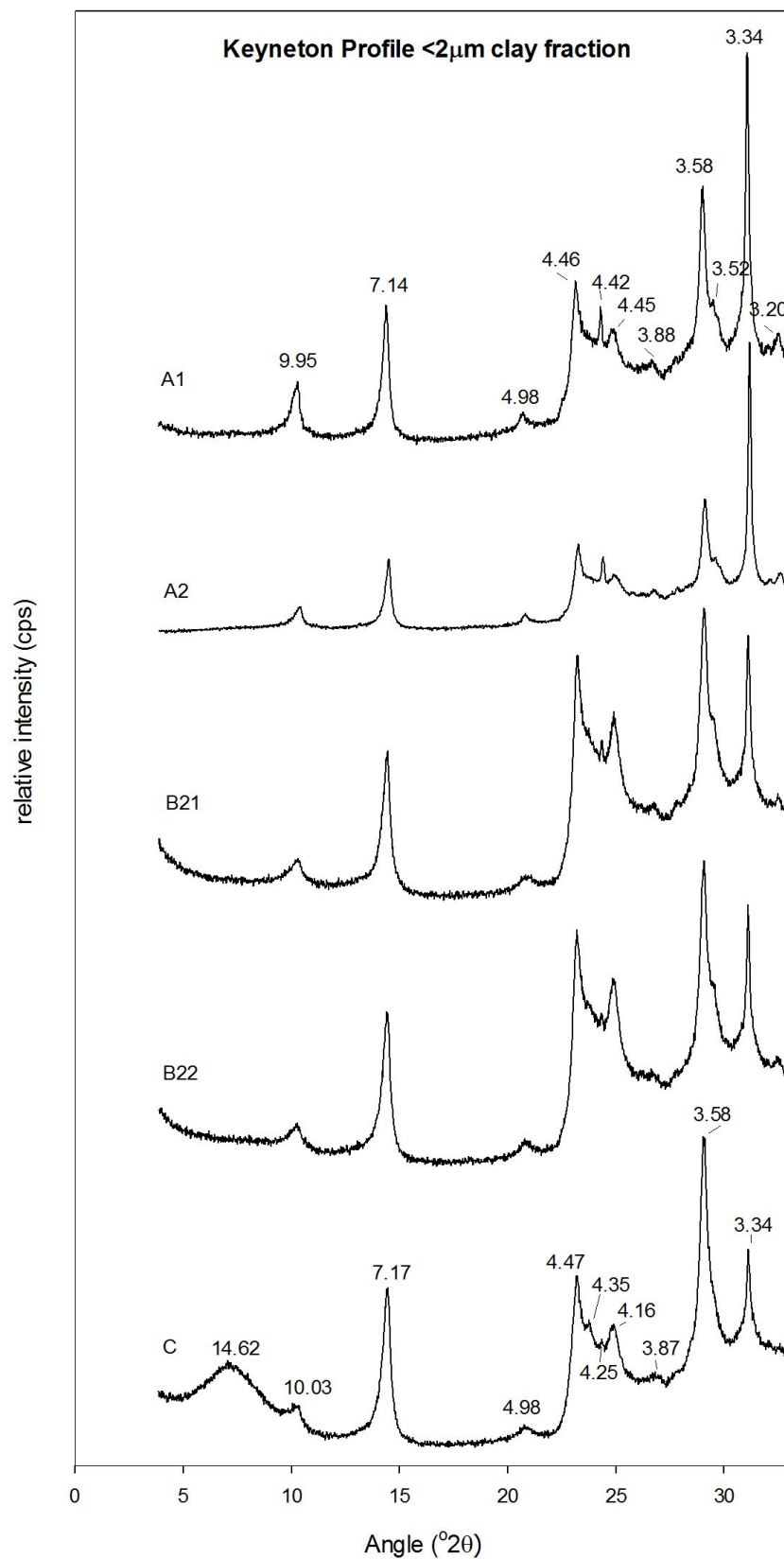
Figure 8: X-ray diffractograms (Fe-filtered CoKα radiation) from the clay fraction (≤2 µm) of the Keyneton soil profile, labelled with corresponding soil horizons. The numerical values assigned to the peaks represent spacing between layers (in Angstroms, 10^{-10} m) that characterise the crystal structure of individual clay minerals.
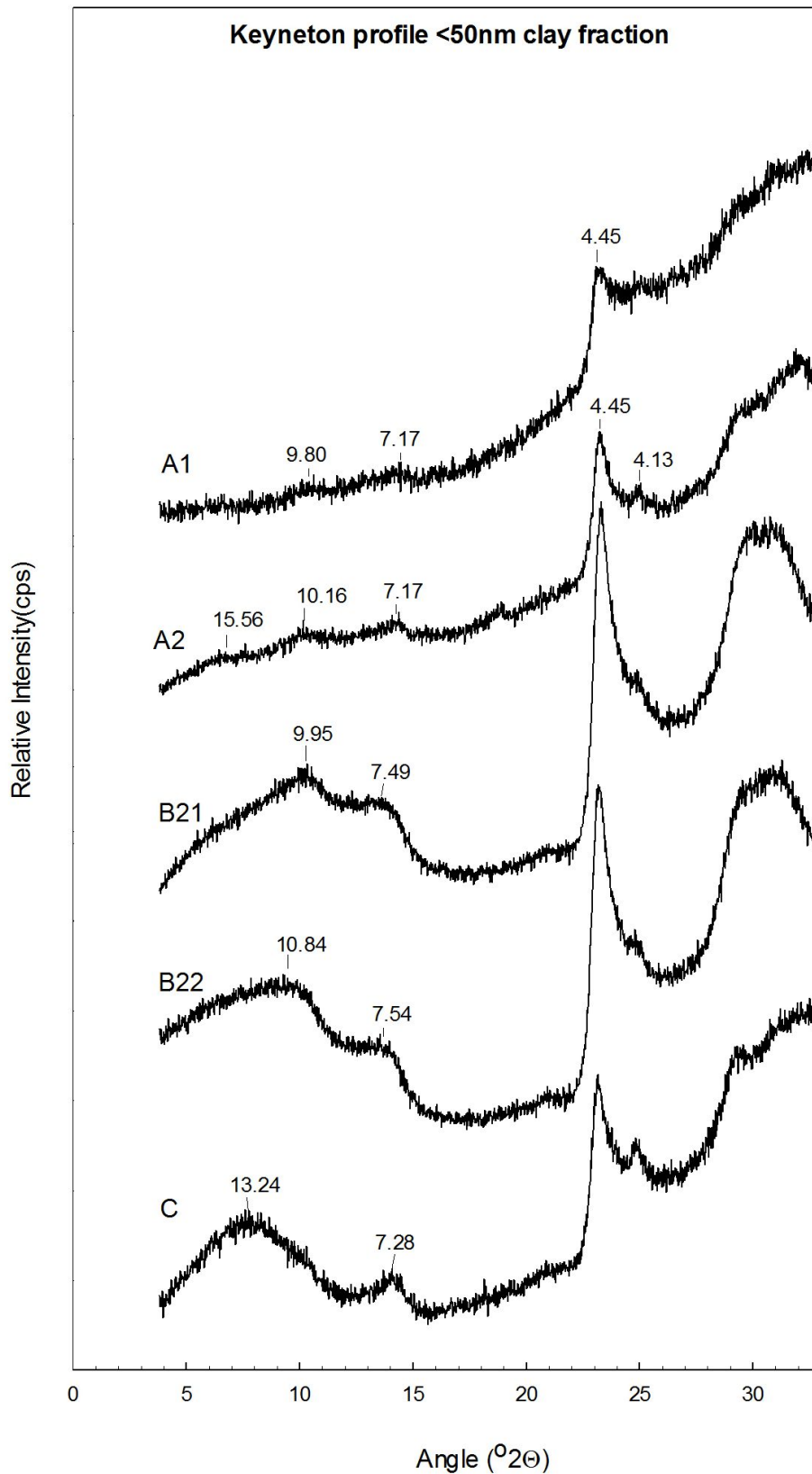
Figure 9: X-ray diffractograms (Fe-filtered CoKα radiation) from the clay fraction (≤50 nm) of the Keyneton soil profile, labelled with corresponding soil horizons. The numerical values assigned to the peaks represent the spacing between layers (in Angstroms, 10^{-10} m) that characterise the crystal structure of individual clay minerals.

Table 2: Quantitative mineralogy from the Keyneton soil profile in various particle size fractions, determined by x-ray diffraction analysis.

Horizon	Depth (cm)	Particle size fraction (μm)	Quartz (wt. %)	Mica (wt. %)	Kaolinite (wt. %)	Plagioclase Feldspar (wt. %)	Alkali Feldspar (wt. %)
A2	8 – 18	2 – 20	40-50	10-20	10-15	10-15	5-10
A2	8 – 18	20 – 63	>80	1-5	1-3	5-10	2-5
B22	33 – 54	2 – 20	25-35	25-35	15-20	5-10	2-5
B22	33 – 54	20 – 63	>75	5-10	1-3	5-10	1-5
R	80 - 100	All	50-70	15-20	10-15	1-3	3-7

Mass balance reconstruction
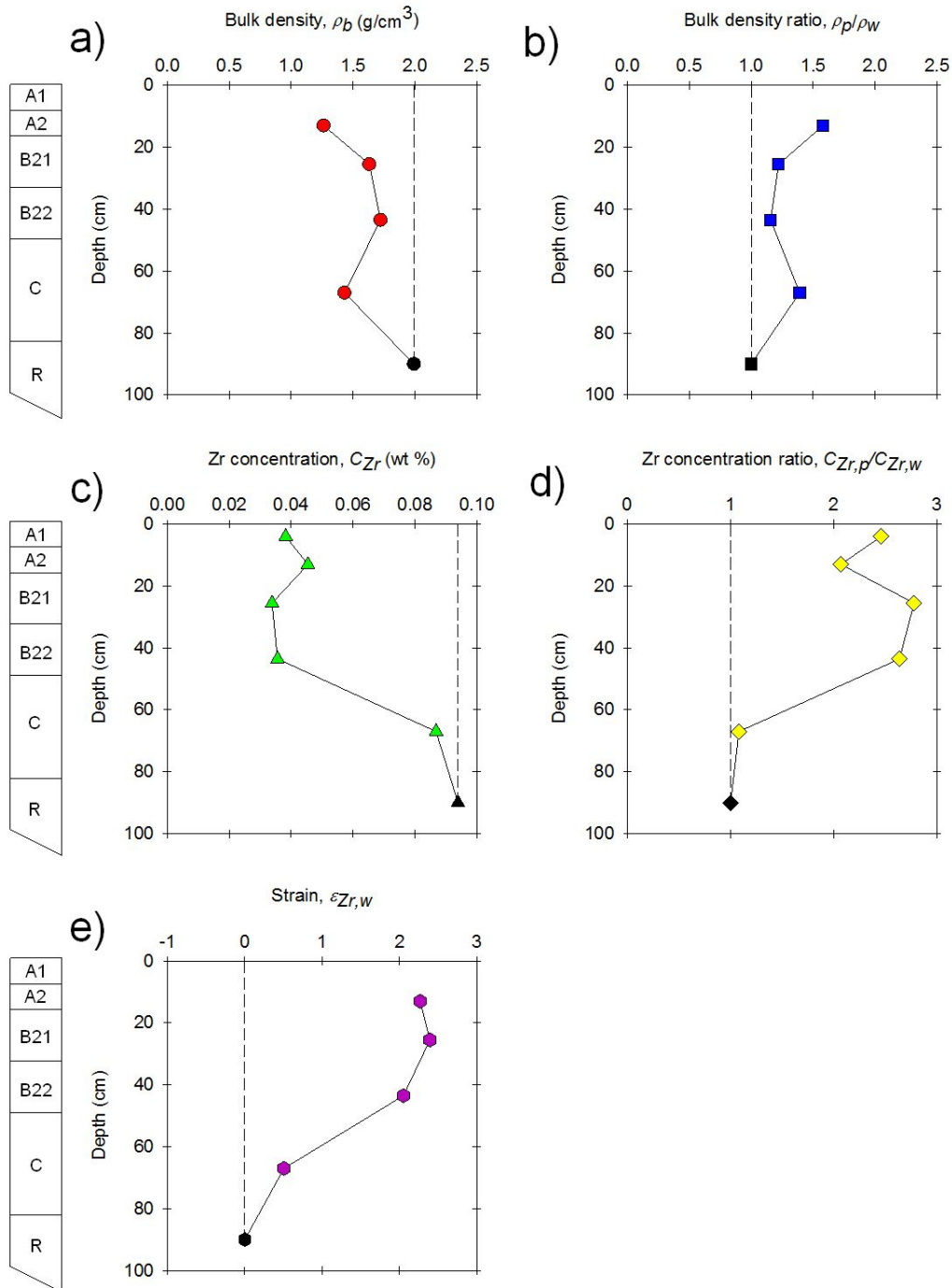
Figure 10: Depth plots of the a) bulk density (g/cm^3), b) bulk density ratio (bulk density of parent material, ρ_p/bulk density of soil horizon, ρ_w), c) concentration of Zr (wt. %), d) Zr depletion factor (concentration of Zr in soil horizon, $C_{Zr,w}$/concentration of Zr in parent material, $C_{Zr,p}$), and e) strain (volume change) using Zr as the immobile index element. Strain represents the fraction of volume gained or lost from the soil profile with respect to the parent material. This figure demonstrates all components of the strain calculation. A strain value of -1 indicates 100% loss of volume (collapse), and a value of +1 indicates 100% gain of volume.
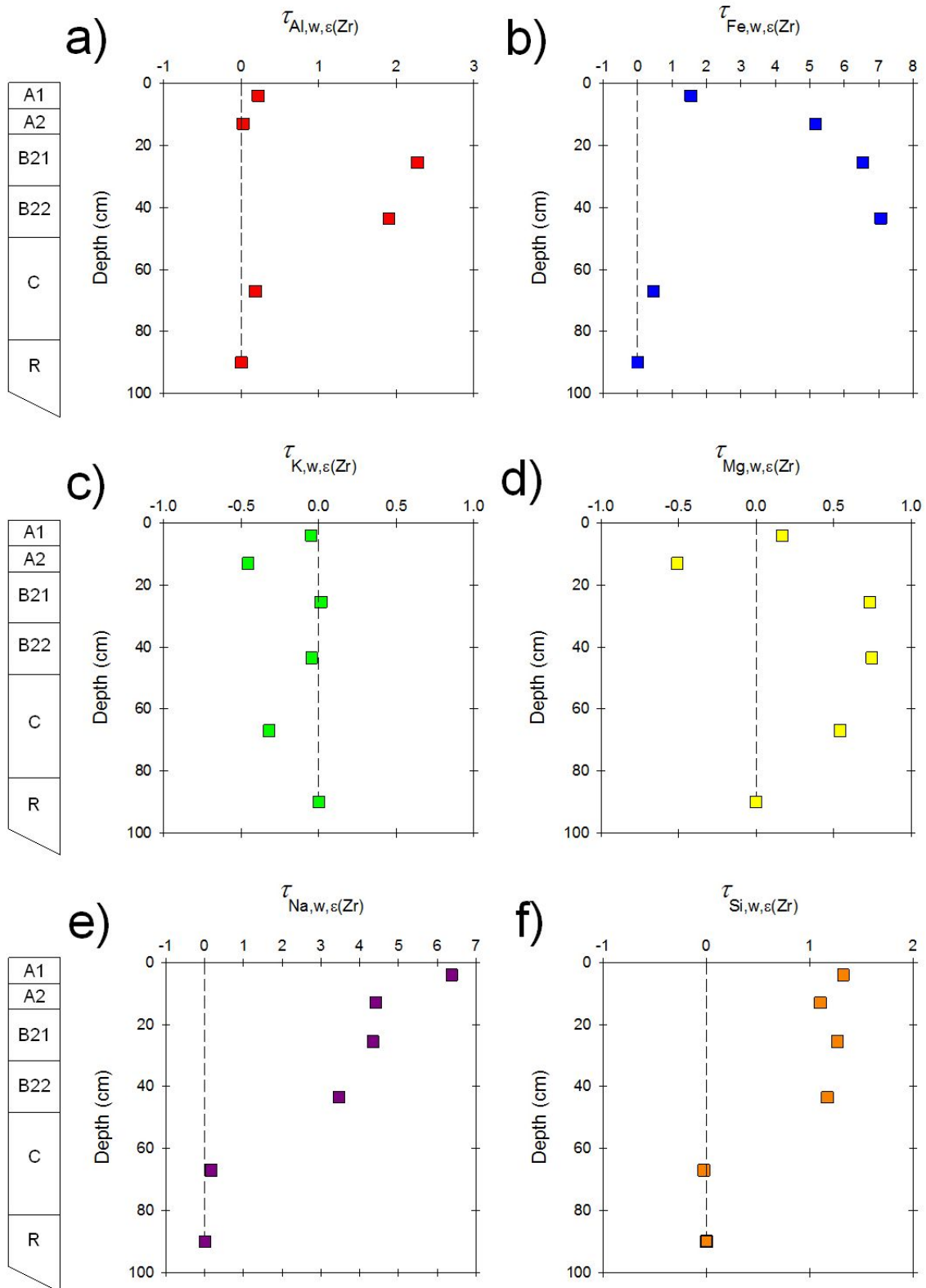
Figure 11: Depth plots of the transported mass fraction ($\tau_{j,w,\varepsilon(Zr)}$) for a) Al, b) Fe, c) K, d) Mg, e) Na, and f) Si from the Keyneton soil profile using Zr as the immobile index element. The transported mass fraction ($\tau_{j,w,\varepsilon(Zr)}$) represents the fraction of an elemental constituent gained or lost relative to the parent material. A transported mass fraction ($\tau_{j,w,\varepsilon(Zr)}$) value of -1 indicates a 100% loss of the constituent while a value of +1 indicates a 100% gain. Note the differences in scale on the x axes.

Table 3: Changes in volume and mass of the Keyneton soil profile due to pedogenesis. These values apply to a section soil profile with volume equal to 1cm^2 multiplied by the depth of the profile (excluding the percentage values). The A1 horizon has been excluded due to weak structure that prevented an accurate bulk density measurement.

Horizon	Present day volume (cm^3)	Parent material volume (cm^3)	Volume change (cm^3)	Volume change (%)	Present day mass m_w (g)	Parent material mass m_p (g)	Mass change Δm (g)	Mass change Δm (%)
A2	10.0	3.1	+6.9	+226.7	12.6	6.1	+6.5	+106.8
B21	15.0	4.4	+10.6	+239.2	24.5	8.8	+15.7	+177.8
B22	21.0	6.9	+14.1	+205.1	36.2	13.7	+22.5	+163.8
C	26.0	17.3	+8.7	+50.6	37.2	34.4	+2.8	+8.2
R	20.0	20.0	+0.0	+0.0	39.8	39.8	+0.0	+0.0
Total	92.0	51.6	+40.4	+78.2	150.2	102.8	+47.4	+46.1
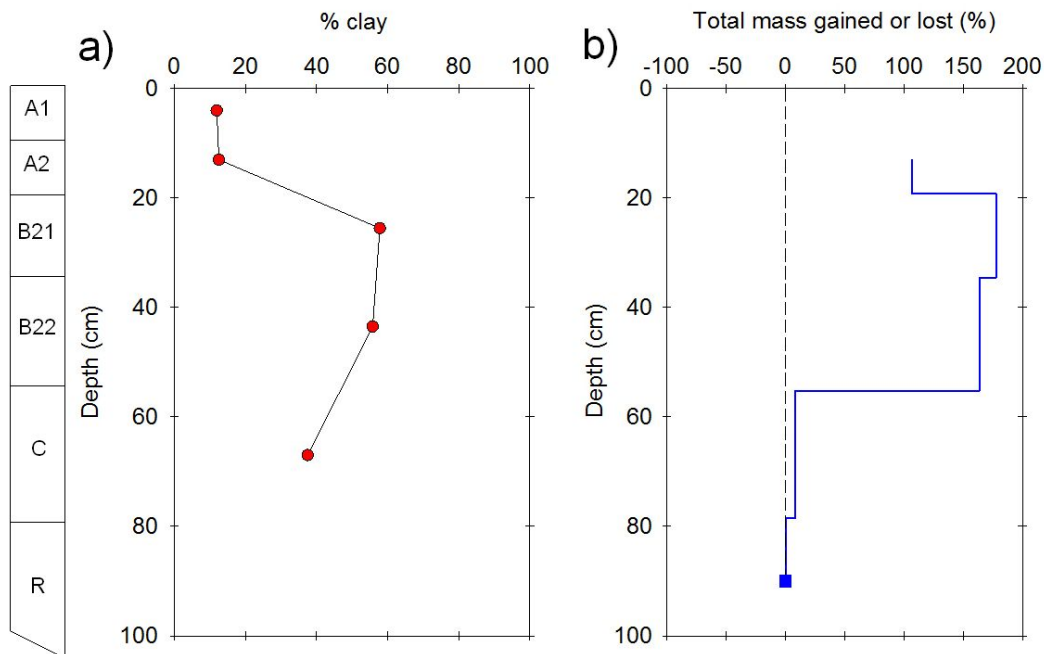
Figure 12: Depth plots of a) percentage clay of the fine earth fraction (≤2000 μm) and b) the total mass gained (%) during pedogenesis of the Keyneton soil profile.

DISCUSSION

Particle size distribution

The particle size distribution of the fine earth fraction (≤2 mm) attained by the hydrometer method (Gee & Or 2002) clearly demonstrates an abrupt textural change between the A2 and B21 horizons (Figure 2), where a dramatic increase in clay is accompanied by a decrease in sand-sized particles across the horizon boundary. This is consistent with the particle size trends of texture contrast soils investigated by Chittleborough & Oades (1979) and Walker & Chittleborough (1986), where clay maxima occur in the B horizons. Although a common practice, there are errors associated with the hydrometer method as it requires the disaggregation of all particles prior to analysis. This cannot be guaranteed; however, the manual grinding of samples and use of chemical dispersing agents in this study minimises this error.

Sieving analysis of the fine earth fraction enabled the proportions of silt-and-sand-sized particles throughout the profile to be quantified (Figure 3). These results support those obtained via the hydrometer method, showing a significant decrease in coarse particles across the A2 and B21 horizon boundary where the significant increase in clay was shown to occur. Ratios of fine to coarse particle size fractions (Figure 4) confirm an increase in the proportion of larger particles towards the surface, indicating that minerals of the silt and fine sand fractions which are susceptible to weathering have been broken down, possibly to clay minerals. If this is the case, it would be reasonable to suggest that the removal of clay from the surface horizons by illuviation or lateral translocation has played a significant role in the formation and development of textural contrast.

When clay is translocated by percolating water, it is often deposited upon the surface of grains and voids, creating argillans (Chittleborough, 1992). Transmitted light micrographs of the B21 and B22 horizons from the Keyneton profile (Figure 5b, c & d) show the presence of argillans (clay coatings) aligned parallel to void and grain surfaces. In the B22 horizon, the argillans are particularly pronounced and distinct laminae are observed. This suggests that the deposition of clay in the subsurface has been episodic, possibly in conjunction with the wet and dry cycles experienced by the soil due to the Mediterranean climate in which has developed. The micrographs leave little doubt that clay deposition in the B horizons has at least contributed to textural differentiation between surface and subsurface; however, the microstructural features alone cannot account for the direction in which the clay originated, or if translocation is the only mechanism responsible for the accumulation.

Evaluation of parent material uniformity

Ratios of elements known to be found primarily within the resistant mineral fraction were used as criteria to assess the uniformity of the parent material from which the Keyneton profile has formed. Elemental ratios are beneficial to investigations as they limit the impact of variations in the total concentration of an element throughout a weathering profile (Marsan et al., 1988).

Figure 6a) shows that there is little variation with depth in the Nd:Zr and Y:Zr ratios from the 20-125 μm fraction, as well as the Nb:Zr ratio from the whole soil fraction. These results meet the requirements of Brewer (1976) who states that there must be little to no variation in the ratios with depth if the parent material is to be considered

uniform. The Zr:Ti ratio does show significant deviation between the A1 and A2 horizons, while remaining relatively constant throughout the remainder of the profile. This variation suggests a possible aeolian mode of origin for the A1 horizon, while the discrepancy could also be attributed to the occurrence of Ti in easily weathered minerals such as biotite and ilmenite. A previous study by Anda *et al*. (2009) has shown that Ti bearing minerals can be weathered to a large extent, providing warning that the Zr:Ti ratio should be used with caution. Given the relative constant nature of the ratios from the Keyneton profile, there is enough evidence to confirm that it has formed from uniform parent material.

Determining the extent & intensity of weathering

Weathering indices are often applied to soil profiles in an effort to quantify the extent of weathering and compare the intensity in different horizons. The chemical index of alteration (CIA) proposed by Nesbitt & Young (1982) has been applied to the Keyneton soil profile as a function of depth (Figure 7). Values of the CIA are expected to be ≤50 for fresh rock, or 100 for heavily weathered material (Nesbitt & Young, 1982). The results suggest significant weathering throughout the entire Keyneton profile, with the greatest degree of weathering occurring in the B horizons. The validity of the CIA is questionable, especially in this instance, given that the relatively unaltered sandstone parent material has a CIA value close to 80, indicating extensive weathering. The CIA assumes immobility of aluminium, a limitation identified by Chittleborough (1991) on the basis that that aluminium is commonly translocated as part of clay minerals. This limitation renders the CIA unreliable for application to the Keyneton profile where evidence of clay translocation abounds.

The degree of weathering indicated by the CIA is also contrary to the physical evidence observed in the transmitted light micrographs of the Keyneton profile. Figure 5 shows a selection of images from surface horizons through to the parent material, with the A2 B21 and B22 horizons showing a markedly greater extent of weathering than the C and R horizons. In particular, the A2 horizon has abundant void space where it is likely that dissolution of weatherable minerals has occurred, being broken down and transported out of the horizon.

Qualitative x-ray diffraction analyses of the ≤2 μm and ≤0.05 μm clay fractions from the Keyneton profile provides identification of clay minerals and allows determination of their location throughout the profile. The ≤2 μm clay fraction (Figure 8) shows prominent peaks representing kaolinite (~15 °2θ, d-spacing: 7.14 Å) and illite (~10 °2θ, d-spacing: 9.95 Å) that are present throughout the profile. The illite peak starts to broaden and become asymmetric in the B21 and B22 horizons, which is characteristic of interstratification with smectite (Moore & Reynolds, 1989). The C horizon has a broad characteristic smectite peak (~7 °2θ, d-spacing: 14.62) that confirms the interstratification with illite. These results suggest that kaolinite and illite have formed as products of weathering in the A1, A2, B21 and B22 horizons, while smectite is formed at the forefront of parent material degradation, in the C horizon. Mineralogy from the ≤0.05 μm clay fraction shows similar results, with the identification of kaolinite and illite in the surface horizons and the presence of illite interstratified with smectite becoming more prominent with increasing depth (Figure 9). In addition to this, interstratification between kaolinite and illite of the ≤0.05 μm fraction occurs in the B21 and B22 horizon.

A complementary quantitative analysis of the mineralogy from the Keyneton soil profile by x-ray diffraction also assists in the interpretation of weathering (Table 2). Throughout the profile, the concentration of quartz is relatively constant due to its resistance to weathering. Interestingly, mica and kaolinite are found in higher concentrations in the B22 horizon as opposed to both the A2 and R horizons. This could be due to a greater intensity of weathering in the B22 horizon, or fine mica and kaolinite could have been deposited in the B22 horizon after originating elsewhere.

Mass balance reconstruction

By investigation of physical and chemical parameters, changes in volume and density during soil formation and weathering processes of the Keyneton profile have been quantified. The bulk density (Figure 10a) decreases significantly up the profile. This indicates an increase in porosity resulting from residual enrichment where dissolution and removal of soluble minerals has led to an increased proportion of coarse, resistant minerals (Chadwick *et al*. 1990). To calculate volume change, Zr was assigned as the immobile index element. This decision was based on the fact that Zr was present in reasonable concentration throughout the profile and that the ratios of Zr to other elements found in resistant minerals indicated that it has not been mobile during soil formation (Figure 6). By combination of the bulk density ratio (Figure 10b) and the Zr concentration ratio (Figure 10d), the strain was quantified.

A large amount of positive strain, or volume change, has taken place in the Keyneton profile (Figure 10e). Strain values of greater than +2 occur in the A2, B21 and B22 horizons, representing increases in volume of greater that 200% per horizon. Volume

change has also occurred in the C horizon with an increase of 50%. Excluding the A1 horizon, a significant cumulative volumetric expansion of 78.2% has occurred throughout the profile (Table 3). These results are similar to those obtained by Jersak *et al*. (1995) who discovered large strain values in three separate soil profiles. Brimhall (1992) suggests that large volume changes can often be a result of bioturbation, with animals and root systems causing expansion. This is an unlikely explanation for the Keyneton profile as vegetation is not dense. Many other mass balance reconstructions, such as those by Chadwick *et al*. (1990) & Driese *et al*. (2000), produced strain values of much smaller proportions. Despite its usefulness, a limitation of this mass balance reconstruction is the inability to determine in which direction strain occurred.

Having calculated the bulk density ratio (Figure 10b) and strain (Figure 10e), the loss or gain of elemental constituents from soil horizons was calculated in the form of the transported mass fraction, outlined by Chadwick *et al*. (1990). The transported mass fractions of Al, Fe, K, Mg, Na, and Si are presented in Figure 11. Gains of up to 200% in Al occur in the B21 and B22 horizons, possibly indicating the accumulation of Al as part of clay minerals that are products of weathering. Fe shows large gains, from 500-700%, in the A2, B21, and B22 horizons. Such large additions suggest an external source of Fe that has possibly contributed to the formation of the ironstone gravel that was observed (Table 1).

The transported mass fractions of K, Mg, Na, and Si are important to soil formation due to their relatively high concentrations in rock-forming minerals (Jersak *et al*. 1995). The Keyneton profile shows losses of K, possibly due to the weathering of both K-feldspar

and microcline; however, given than K is a common plant nutrient, it is also possible that plants have extracted K from the soil, with their degradation products removed from the surface by erosion or water transport, without returning to the soil. Mg is lost from the A2 horizon, but gained in the B21 and B22 horizons, which may indicate the weathering and re-deposition of mica minerals. The A1, A2, B21, and B22 horizons all show large gains of Na and Si, to such an extent that an external atmospheric source is likely for their origin.

Implications for soil development

The Keyneton profile has undergone significant volumetric expansion of 78.2% and increased in mass by 46.1% when compared to its parent material precursor (Table 3). These changes are significant, with the largest changes in volume and mass evident in the B horizons. This also coincides with a large increase in clay content in the B horizons, indicating that the accumulation of clay in the subsurface has played a large role in volume and mass expansion (Figure 12).

Given the extent of the changes, it is possible that there is more to the development of the Keyneton profile than just pedological processes. During soil formation, a greater intensity of weathering at the surface resulted in the observed coarse A horizons. If the thickness of the A horizons was originally much greater, the high porosity would have resulted in a low water holding capacity which, in turn, would have depleted vegetation during summer when drying of the upper profile would have been extensive. With little to no cover, the coarse A horizons could have been eroded to their relatively small present-day thickness. When considering scenarios of profile development like this, a

limitation of the mass balance reconstruction technique is evident, with geological processes such as surface erosion unable to be accounted for.

CONCLUSIONS

Strong texture contrast between surface and subsurface soil horizons is a prevalent feature in many localities around the world. Despite common occurrence, a definitive explanation for the formation and development of this characteristic is yet to be elucidated. Inheritance of textural stratification from parent material, clay translocation, differential weathering between soil horizons, and bioturbation have all been noted as potential contributing factors. The Keyneton soil profile, like many texture contrast soils, has been shown to exhibit a dramatic increase in clay content between A and B horizons. Constant resistant mineral ratios throughout the profile indicate that the abrupt textural change is a result of pedogenic processes, rather that geologic inheritance. Weathering indices, x-ray diffraction analysis, and microstructural evidence suggest that weathering has been greater in the surface horizons, with large amounts of clay accumulating in the subsurface. Mass balance calculations show that the profile has been subject to significant volumetric expansion with the addition of large quantities of Al, Fe, Si, and Na contributing to a large cumulative mass gain. Although mass balance analyses are limited to the quantification of pedological processes, the correlated clay and mass increases in the B horizons are strong evidence that clay translocation has been a dominant process in textural differentiation.

ACKNOWLEDGMENTS

REFERENCES (LEVEL 1 HEADING)

ANDA M., CHITTLEBOROUGH D. J. & FITZPATRICK R. W. 2009. Assessing parent material uniformity of a red and black soil complex in the landscapes. *Catena* **78**, 142-153.

BEAVERS A., FEHRENBACHER J., JOHNSON P. & JONES R. L. 1963. CaO-ZrO2 molar ratios as an index of weathering. *Soil Science Society of America Journal* **27**, 408-412.

BISHOP P., MITCHELL P. & PATON T. 1980. The formation of duplex soils on hillslopes in the Sydney Basin, Australia. *Geoderma* **23**, 175-189.

BREWER R. 1976. Fabric and Mineral Analysis of Soils Krieger. *Huntington, NY*, 482.

BRIMHALL G. H., CHADWICK O. A., LEWIS C. J., COMPSTON W., WILLIAMS I. S., DANTI K. J., DIETRICH W. E., POWER M. E., HENDRICKS D. & BRATT J. 1992. Deformational mass transport and invasive processes in soil evolution. *Science* **255**, 695-702.

BRIMHALL G. H., CHRISTOPHER J L., FORD C., BRATT J., TAYLOR G. & WARIN O. 1991. Quantitative geochemical approach to pedogenesis: importance of parent material reduction, volumetric expansion, and eolian influx in lateritization. *Geoderma* **51**, 51-91.

BRIMHALL G. H. & DIETRICH W. E. 1987. Constitutive mass balance relations between chemical composition, volume, density, porosity, and strain in metasomatic hydrochemical systems: Results on weathering and pedogenesis. *Geochimica et Cosmochimica Acta* **51**, 567-587.

BRIMHALL G. H., LEWIS C. J., AGUE J. J., DIETRICH W. E. & HAMPEL J. 1988. chemically mature aeolian dust. *Nature* **333**, 30.

CARTER M. R. 1993. *Soil sampling and methods of analysis*. CRC Press.

CHADWICK O. A., BRIMHALL G. H. & HENDRICKS D. M. 1990. From a black to a gray box—a mass balance interpretation of pedogenesis. *Geomorphology* **3**, 369-390.

CHITTLEBOROUGH D. 1991. Indices of weathering for soils and palaeosols formed on silicate rocks. *Australian Journal of Earth Sciences* **38**, 115-120.

CHITTLEBOROUGH D. 1992. Formation and pedology of duplex soils. *Animal Production Science* **32**, 815-825.

CHITTLEBOROUGH D. & OADES J. 1979. The development of a red-brown earth. I. A reinterpretation of published data. *Soil Research* **17**, 371-381.

CHITTLEBOROUGH D. & OADES J. 1980. The development of a red-brown earth. II. Uniformity of the parent material. *Soil Research* **18**, 375-382.

CHITTLEBOROUGH D. & OADES J. 1980. The development of a red-brown earth. II. Uniformity of the parent material. *Soil Research* **18**, 375-382.

CHITTLEBOROUGH D., OADES J. & WALKER P. 1984. Textural differentiation in chronosequences from eastern Australia, III. Evidence from elemental chemistry. *Geoderma* **32**, 227-248.

CHITTLEBOROUGH D., WALKER P. & OADES J. 1984. Textural differentiation in chronosequences from eastern Australia, I. Descriptions, chemical properties and micromorphologies of soils. *Geoderma* **32**, 181-202.

CHITTLEBOROUGH D., WALKER P. & OADES J. 1984. Textural differentiation in chronosequences from eastern Australia, II. Evidence from particle-size distributions. *Geoderma* **32**, 203-226.

DRIESE S. G., MORA C. I., STILES C. A., JOECKEL R. & NORDT L. C. 2000. Mass-balance reconstruction of a modern Vertisol: implications for interpreting the geochemistry and burial alteration of paleo-Vertisols. *Geoderma* **95**, 179-204.

FITZPATRICK R. W., RILEY, T.W., WRIGHT, M.J. & FIELKE, J.M. 1990. Distribution, classification and properties of the abrasiveness of Australian soils. *Highly abrasive soils and ground engaging tool performance.*

GATEHOUSE C. G., JAGO J. B. & COOPER B. J. 1990. Sedimentology and stratigraphy of the Carrickalinga Head Formation (low stand fan to high stand systems tract), Kanmantoo Group, South Australia. *The Evolution of a Late Precambrian–Early Palaeozoic Rift Complex: the Adelaide Geosyncline*, 351-368.

GEE G. W. & OR D. 2002. 2.4 Particle-size analysis. *Methods of Soil Analysis: Physical Methods* **5**, 255.

GROSSMAN R. & REINSCH T. 2002. Bulk density and linear extensibility. *Methods of soil analysis. Part* **4**, 201-228.

HARNOIS L. 1988. The CIW index: A new chemical index of weathering. *Sedimentary Geology* **55**, 319-322.

HECKMAN K. & RASMUSSEN C. 2011. Lithologic controls on regolith weathering and mass flux in forested ecosystems of the southwestern USA. *Geoderma* **164**, 99-111.

ISBELL R. F. 1996. *The Australian Soil Classification*. CSIRO Publishing, Melbourne, Australia.

JAGO J. B., GUM J. C., BURTT A. & HAINES P. W. 2003. Stratigraphy of the Kanmantoo Group: a critical element of the Adelaide Fold Belt and the Palaeo-Pacific plate margin, Eastern Gondwana. *Australian Journal of Earth Sciences* **50**, 343-363.

JERSAK J., AMUNDSON R. & BRIMHALL G. 1995. A mass balance analysis of podzolization: examples from the northeastern United States. *Geoderma* **66**, 15-42.

JOHNSON D. L. 1990. Biomantle evolution and the redistribution of earth materials and artifacts. *Soil Science* **149**, 84.

KLAMINDER J. & YOO K. 2008. Contaminants as tracers for studying dynamics of soil formation: mining an ocean of opportunities. *Advances in Agronomy* **100**, 15-57.

KRULL E. S., BESTLAND E. A., SKJEMSTAD J. O. & PARR J. F. 2006. Geochemistry (? 13C,? 15N, 13C NMR) and residence times (14C and OSL) of soil organic matter from red-brown earths of South Australia: Implications for soil genesis. *Geoderma* **132**, 344-360.

MARSAN F. A., BAIN D. & DUTHIE D. 1988. Parent material uniformity and degree of weathering in a soil chronosequence, northwestern Italy. *Catena* **15**, 507-517.

MCMASTER J. S. 1992. Qualitative soil survey and land capability assessment of the Keynes Catchment, Keyneton, South Australia. Master of Agriculture in Soil Conservation thesis, Department of Soil Science, The University of Adelaide, Adelaide (unpubl.).

MOORE D. M. & REYNOLDS JR R. C. 1989. *X-ray diffraction and the identification and analysis of clay minerals*. Oxford University Press (OUP).

NESBITT H. & YOUNG G. 1982. Early Proterozoic climates and plate motions inferred from major element chemistry of lutites. *Nature* **299**, 715-717.

NETTLETON W., FLACH K. & BRASHER B. 1969. Argillic horizons without clay skins. *Soil Science Society of America Journal* **33**, 121-125.

NOOREN C., VAN BREEMEN N., STOORVOGEL J. & JONGMANS A. 1995. The role of earthworms in the formation of sandy surface soils in a tropical forest in Ivory Coast. *Geoderma* **65**, 135-148.

NORTHCOTE K. 1979. A Factual Key for the Recognition of Australian Soils, 4th Edn, Rellim Tech. *Publications, Glenside, SA*.

OERTEL A. 1974. The development of a typical red-brown earth. *Soil Research* **12**, 97-105.

PHILLIPS J. D. 2001. Contingency and generalization in pedology, as exemplified by texture-contrast soils. *Geoderma* **102**, 347-370.

PHILLIPS J. D. 2004. Geogenesis, pedogenesis, and multiple causality in the formation of texture-contrast soils. *Catena* **58**, 275-295.

SMECK N., TORRENT J. & BARRÓN V. 1994. Genesis and native phosphorus distribution in some Palexeralfs of southern Spain. *Soil Science Society of America Journal* **58**, 1718-1723.
STACE H. C. T., HUBBLE, G.D., BREWER, R., NORTHCOTE, K.H., SLEEMAN, J.R., MUCAHY, M.J. & HALLSWORTH, E.G. 1968. *A Handbook of Australian Soils*. Rellim Technical Publications, Glenside, South Australia.
SOIL SURVEY STAFF 1999. *Soil taxonomy: A basic system of soil classification for making and interpreting soil surveys* (2nd edition). USDA: Natural Resources Conservation Service.
SOIL SURVEY STAFF 2010. *Keys to soil taxonomy* (11th edition). USDA: Natural Resources Conservation Service.

APPENDIX A: FIELD METHODS

The Keyneton soil profile sampled for this study was located 65 km northeast of Adelaide on the eastern flank of the Mount Lofty Ranges, South Australia (Figure 1). The site was found at latitude 34° 32' 5" S and longitude 139° 8' 30" E. Soils of the local area are predominantly Alfisols (Soil Survey Staff, 1999; 2010), with the sampled profile further classified as a Natric Palexeralf (Fitzpatrick *et al*. 1990; Soil Survey Staff 1999, 2010).

An excavator was used to dig a pit of approximately 1.6 m depth on a section of undisturbed native land, adjacent to paddocks that had been previously cleared for agricultural purposes. Soil horizons were assigned and described in the field by observation. Representative bulk samples of ~800 g, or enough to fill a 20 cm x 30 cm plastic zip-lock bag, were collected from each horizon by hand and with the use of a pick. Four intact clods of each horizon, approximately fist-sized, were taken from the face of the excavation and stored carefully in cotton wool and plastic bags to ensure the structure of the samples was retained.

A monolith of the sampled profile stored at the University of Adelaide's Waite campus was used to provide a profile photograph.
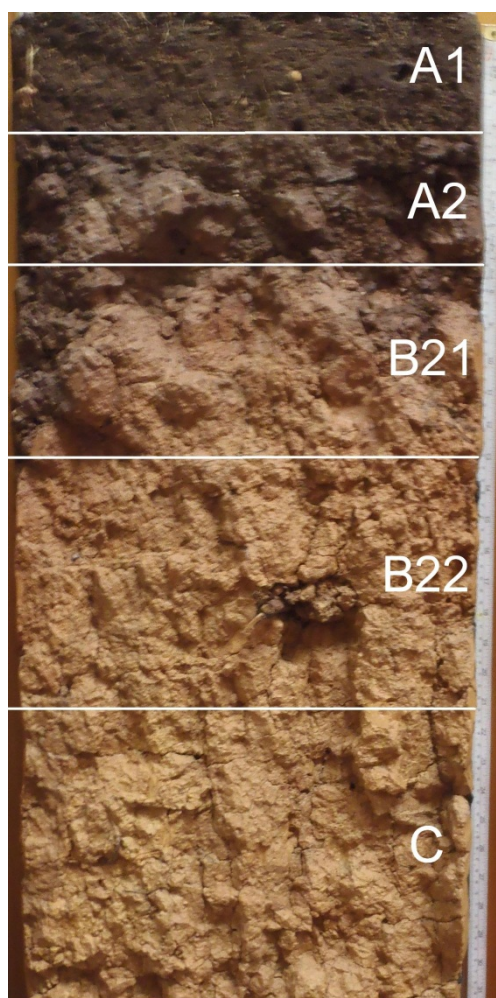
Figure 13: Photograph of the Keyneton profile monolith with horizons marked.

APPENDIX B: PARTICLE SIZE ANALYSIS

Hydrometer method

The particle size distribution of the Keyneton profile was obtained using the hydrometer method outlined by Gee & Or (2002).

Particle sizes were identified by: clay ($\leq$2 μm), silt (2-20 μm), and sand (20-2000 μm).

The exact details of the method followed are described below:

Apparatus:
Mortar & pestle
2mm diameter sieve
Top-weighing laboratory balance
6 x 400 ml cylindrical plastic screw-cap containers
5 ml volumetric pipette
10 ml volumetric pipette
End-over-end shaker
6 x 1L measuring cylinders
Mixing rod

Materials:
Oven-dry soil (~70 g from each sampling horizon)
10% sodium tripolyphosphate (60 ml)
1N sodium hydroxide
Deionised water

Procedure:
1. ~70 g of soil from each sampling horizon (A1, A2, B21, B22, C) was placed in an oven at 42°C for 24 hours. The weight of each oven-dried sample was recorded.
2. The oven-dry samples were ground using a mortar & pestle to separate particles.
3. The material from each sampling horizon was passed through a 2 mm sieve. The weight of both the fine earth fraction (<2 mm) and the gravel fraction (>2 mm) were recorded and the % gravel calculated.
4. ~50 g of oven-dry material from the fine-earth fraction (<2 mm) of each horizon were added to individual 400 ml cylindrical plastic screw cap containers.
5. 10 ml 10% sodium tripolyphosphate and 5 ml 1N sodium hydroxide were added to the material in each container. Deionised water was used to make the volume up to 200 ml.
6. A 'blank' solution containing only 10 ml 10% sodium tripolyphosphate, 5 ml 1N sodium hydroxide and 185 ml deionised water was also made up.
7. The 'blank' and the five suspensions were dispersed for 20 hours on an end-over-end shaker.
8. The contents of each container were transferred to individual 1L measuring cylinders and the volumes were made up to the 1L mark with deionised water.

9. The 'blank' was mixed with a mixing rod and the hydrometer was lowered into the solution and the scale reading (R_L) was obtained from the upper edge of the meniscus.
10. All soil suspensions were mixed well with a mixing rod. The time of sedimentation commencement was noted upon removal of the rod.
11. The hydrometer was carefully placed into each soil suspension after the commencement of sedimentation at the following time intervals: 0.5 min, 1 min, 3 min, 10 min, 30 min, 90 min, 270 min, 510 min, 900 min, and 1440 min. Hydrometer readings (R) were recorded at each time interval with the measurement read from the top of the meniscus. Cloth was placed over the cylinders to prevent when they were left for long periods to prevent the entry of atmospheric dust.
12. For each hydrometer reading (R), the concentration of the suspension (C) in g.L^{-1} was calculated from the equation:

$$C = R - R_L$$

Where R_L is the scale reading obtained from the 'blank' solution.

The summation percentage (P) was then calculated from the equation:

$$P = 100(C/C_O)$$

Where C_O was the weight of the oven-dry soil from the fine earth fraction (<2 mm) used in the suspension (in grams).

The corresponding equivalent spherical diameters (in metres), D, was calculated from the equation:

$$D = \theta/t^{0.5}$$

Where t was the sedimentation time in seconds, and θ was the sedimentation parameter.
13. P was plotted against $\log_{10}D$, with D expressed in µm, to provide a summation % curve.
14. From the curve, it was interpolated where D = 2, 5, 20, 50, and 100 µm. The percentage of each particle size fraction was then deduced from this.
15. Steps 12 – 14 were completed for each horizon and textures assigned using the Australian Soil Texture Triangle.

Table 4: Hydrometer readings (R) of soil suspensions at various times after the commencement of sedimentation.

Horizon	R 0.5 min	R 1 min	R 3 min	R 10 min	R 30 min	R 90 min	R 270 min	R 510 min	R 900 min	R 1440 min
A1	28	26	20	18	11.5	9	8	8	7	7
A2	27	22	18	13	11	10.5	9.5	9	8.5	8
B21	46	44	41.5	38	37	36.5	36	36	35.5	35
B22	43	40.5	39	36	35	34	33.5	33	33	32
C	42.5	38.5	33	29	26	24.5	22	21.5	21	20

Table 5: Concentration, C, (g.$^{L-}$1) of soil suspensions at various times after the commencement of sedimentation.

Horizon	C (g.L^{-1}) 0.5 min	C (g.L^{-1}) 1 min	C (g.L^{-1}) 3 min	C (g.L^{-1}) 10 min	C (g.L^{-1}) 30 min	C (g.L^{-1}) 90 min	C (g.L^{-1}) 270 min	C (g.L^{-1}) 510 min	C (g.L^{-1}) 900 min	C (g.L^{-1}) 1440 min
A1	27	25	19	17	10.5	8	7	7	6	6
A2	26	21	17	12	10	9.5	8.5	8	7.5	7
B21	45	43	40.5	37	36	35.5	35	35	34.5	34
B22	42	39.5	38	35	34	33	32.5	32	32	31
C	41.5	37.5	32	28	25	23.5	21	20.5	20	19

Table 6: Summation percentage, P, of soil suspensions at various times after the commencement of sedimentation.

Horizon	C$_O$ (g)	P 0.5 min	P 1 min	P 3 min	P 10 min	P 30 min	P 90 min	P 270 min	P 510 min	P 900 min	P 1440 min
A1	56.27	47.98	44.43	33.77	30.21	18.66	14.22	12.44	12.44	10.66	10.66
A2	59.15	43.96	35.50	28.74	20.29	16.91	16.06	14.37	13.52	12.68	11.83
B21	60.30	74.63	71.31	67.16	61.36	59.70	58.87	58.04	58.04	57.21	56.38
B22	57.60	72.92	68.58	65.97	60.76	59.03	57.29	56.42	55.56	55.56	53.82
C	53.88	77.02	69.60	59.39	51.97	46.40	43.62	38.98	38.05	37.12	35.26

Table 7: Sedimentation parameter, θ, (m.s$^{0.5}$) of soil suspensions at various times after the commencement of sedimentation

Horizon	θ (m.s$^{0.5}$) 0.5 min	θ (m.s$^{0.5}$) 1 min	θ (m.s$^{0.5}$) 3 min	θ (m.s$^{0.5}$) 10 min	θ (m.s$^{0.5}$) 30 min	θ (m.s$^{0.5}$) 90 min	θ (m.s$^{0.5}$) 270 min	θ (m.s$^{0.5}$) 510 min	θ (m.s$^{0.5}$) 900 min	θ (m.s$^{0.5}$) 1440 min
A1	0.000388	0.000392	0.000408	0.000411	0.000425	0.000431	0.000434	0.000434	0.000435	0.000435
A2	0.000390	0.000402	0.000411	0.000422	0.000427	0.000428	0.000430	0.000430	0.000432	0.000434
B21	0.000344	0.000348	0.000353	0.000362	0.000366	0.000367	0.000368	0.000368	0.000369	0.000370
B22	0.000350	0.000358	0.000362	0.000368	0.000371	0.000373	0.000374	0.000374	0.000374	0.000378
C	0.000351	0.000361	0.000376	0.000386	0.000392	0.000395	0.000402	0.000404	0.000406	0.000407

Table 8: Equivalent spherical diameters, D, (μm) of soil suspensions at various times after the commencement of sedimentation

Horizon	D (μm) 0.5 min	D (μm) 1 min	D (μm) 3 min	D (μm) 10 min	D (μm) 30 min	D (μm) 90 min	D (μm) 270 min	D (μm) 510 min	D (μm) 900 min	D (μm) 1440 min
A1	70.84	50.61	30.41	16.78	10.02	5.87	3.41	2.48	1.87	1.48
A2	71.20	51.90	30.63	17.23	10.06	5.82	3.38	2.46	1.86	1.48
B21	62.81	44.93	26.31	14.78	8.63	4.99	2.89	2.10	1.59	1.26
B22	63.90	46.22	26.98	15.02	8.74	5.08	2.94	2.14	1.61	1.29
C	64.08	46.60	28.03	15.76	9.24	5.38	3.16	2.31	1.75	1.38

Table 9: $\log_{10}D$ (where D is the equivalent spherical diameters expressed in µm) of soil suspensions at various times after the commencement of sedimentation

Horizon	$\log_{10}D$ 0.5 min	$\log_{10}D$ 1 min	$\log_{10}D$ 3 min	$\log_{10}D$ 10 min	$\log_{10}D$ 30 min	$\log_{10}D$ 90 min	$\log_{10}D$ 270 min	$\log_{10}D$ 510 min	$\log_{10}D$ 900 min	$\log_{10}D$ 1440 min
A1	1.85	1.70	1.48	1.22	1.00	0.77	0.53	0.39	0.27	0.17
A2	1.85	1.72	1.49	1.24	1.00	0.77	0.53	0.39	0.27	0.17
B21	1.80	1.65	1.42	1.17	0.94	0.70	0.46	0.32	0.20	0.10
B22	1.81	1.66	1.43	1.18	0.94	0.71	0.47	0.33	0.21	0.11
C	1.81	1.67	1.45	1.20	0.97	0.73	0.50	0.36	0.24	0.14
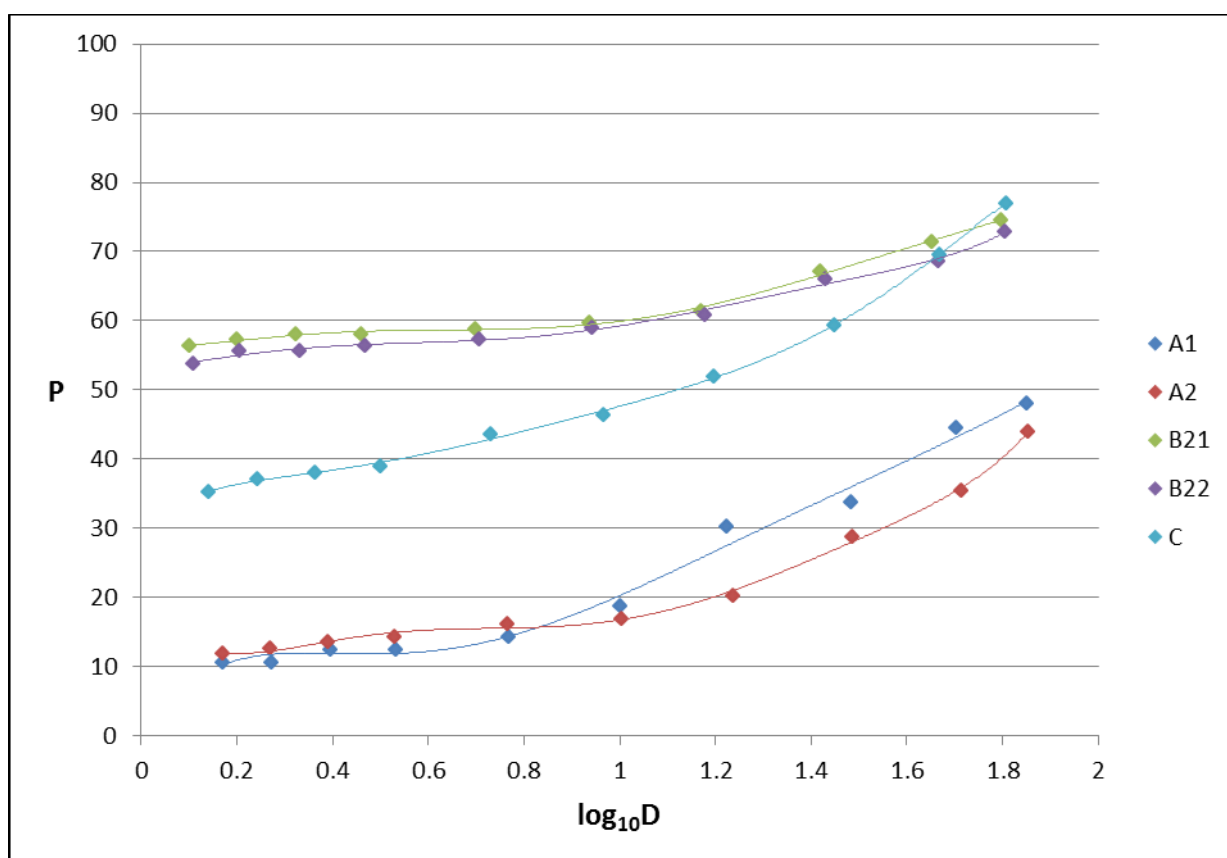
Figure 14: Summation percentage curves for each horizon of the Keyneton profile.

Table 10: Proportions of particle sizes from the Keyneton profile, as determined by the hydrometer method.

Horizon	≤ 2 μm (%)	≤ 5 μm (%)	≤ 20 μm (%)	≤ 50 μm (%)	≤ 100 μm (%)	≤ 2000 μm (%)
A1	11.89	13.22	30.02	42.95	53.67	100
A2	12.53	15.48	22.65	35.21	60.97	100
B21	57.76	58.68	64.24	72.56	79.25	100
B22	55.76	57.13	63.39	69.71	85.83	100
C	37.44	42.36	54.43	71.23	83.43	100

Table 11: Particle size fractions of clay (≤2 μm), silt (2 - 20μm) and sand (20 – 2000 μm) from the Keyneton profile, as determined by the hydrometer method.

Horizon	≤ 2 μm (%)	2 - 20 μm (%)	20 - 2000 μm (%)
A1	11.89	18.12	69.98
A2	12.53	10.12	77.35
B21	57.76	6.48	35.76
B22	55.76	7.64	36.61
C	37.44	16.99	45.57

Analysis by sieving

In addition to the hydrometer method of particle size analysis, wet sieving was carried out with size fractions determined by weight.

Sieve sizes used were: 2000 μm, 250 μm, 125 μm, and 63μm. The <63 μm size fractions were separated by settling times calculated by Stokes' law. Apart from the >2000 μm size fraction, all sieving was carried out in deionised water. Sieving (duration 3 minutes) was carried out for each of the particle size separations.

Table 12: Particle size fractions weights (g) from each horizon of the Keyneton profile, as determined by sieving analysis.

Horizon	Total oven-dried sample (g)	Gravel fraction (>2000 μm) (g)	Fine earth fraction (<2000 μm) (g)	Coarse sand fraction (250-2000 μm) (g)	Fine sand fraction (125-250 μm) (g)	Very fine sand fraction (63-125 μm) (g)	Silt fraction (20-63 μm) (g)	Fine silt fraction (2-20 μm) (g)	Clay fraction (<2 μm) (g)
A1	57.02	0.42	56.27	8.46	6.65	12.60	10.17	7.20	11.19
A2	73.90	14.56	59.15	6.32	6.17	22.00	10.88	3.94	9.84
B21	68.31	7.75	60.30	4.21	2.47	9.31	5.93	2.75	35.63
B22	73.65	15.76	57.60	3.70	2.94	9.91	5.73	3.30	32.02
C	63.45	9.32	53.88	1.21	2.17	12.08	10.51	6.23	21.68

Table 13: Particle size fractions from each horizon of the Keyneton profile, expressed as percentages of the fine earth fraction (≤2000 μm).

Horizon	Fine earth fraction (< 2000 μm) (%)	Coarse sand fraction (250 - 2000 μm) (%)	Fine sand fraction (125 - 250 μm) (%)	Very fine sand fraction (63 - 125 μm) (%)	Silt fraction (20 - 63 μm) (%)	Fine silt fraction (2 - 20 μm) (%)	Clay fraction (<2 μm) (%)
A1	100	15.03	11.82	22.39	18.07	12.80	19.89
A2	100	10.68	10.43	37.19	18.39	6.66	16.65
B21	100	6.98	4.10	15.44	9.83	4.56	59.09
B22	100	6.42	5.10	17.20	9.95	5.73	55.60
C	100	2.25	4.03	22.42	19.51	11.56	40.23

APPENDIX C: THIN SECTIONING & PETROLOGICAL MICROSCOPY

Thin sectioning

Subsamples (approximately 1.5 cm^3) of each soil horizon (A2, B21, B22, C, and R) were taken from intact clods and sent to Earthslides (UK) for hardening and thin sectioning. The samples were de-watered carefully by acetone replacement, following which the samples were impregnated with Polylite Clear Casting Resin and cut with the Multi-Grinder Thin-Section Machine provided by Brot Technologies, working on a vertical axis with fixed diamond wheels. The thin sections were hand-finished to 25 – 30 µm thickness with fixed abrasive silicon carbon papers and sealed with a glass cover slip.

Petrological microscopy

The Nikon LV100 POL petrographic microscopy at Adelaide Microscopy was used for examination of thin sections. Transmitted cross-polarised light was used across a range of magnifications to examine the microstructural features of the soil.

Figure 15: Transmitted cross-polarised light micrograph from the A2 horizon of the Keyneton profile.

Figure 16: Transmitted cross-polarised light micrograph from the A2 horizon of the Keyneton profile.

Figure 17: Transmitted cross-polarised light micrograph from the B21 horizon of the Keyneton profile.

Figure 18: Transmitted cross-polarised light micrograph from the B21 horizon of the Keyneton profile.

Figure 19: Transmitted cross-polarised light micrograph from the B22 horizon of the Keyneton profile.

Figure 20: Transmitted cross-polarised light micrograph from the B22 horizon of the Keyneton profile.

Figure 21: Transmitted cross-polarised light micrograph from the B22 horizon of the Keyneton profile.

Figure 22: Transmitted cross-polarised light micrograph from the B22 horizon of the Keyneton profile.
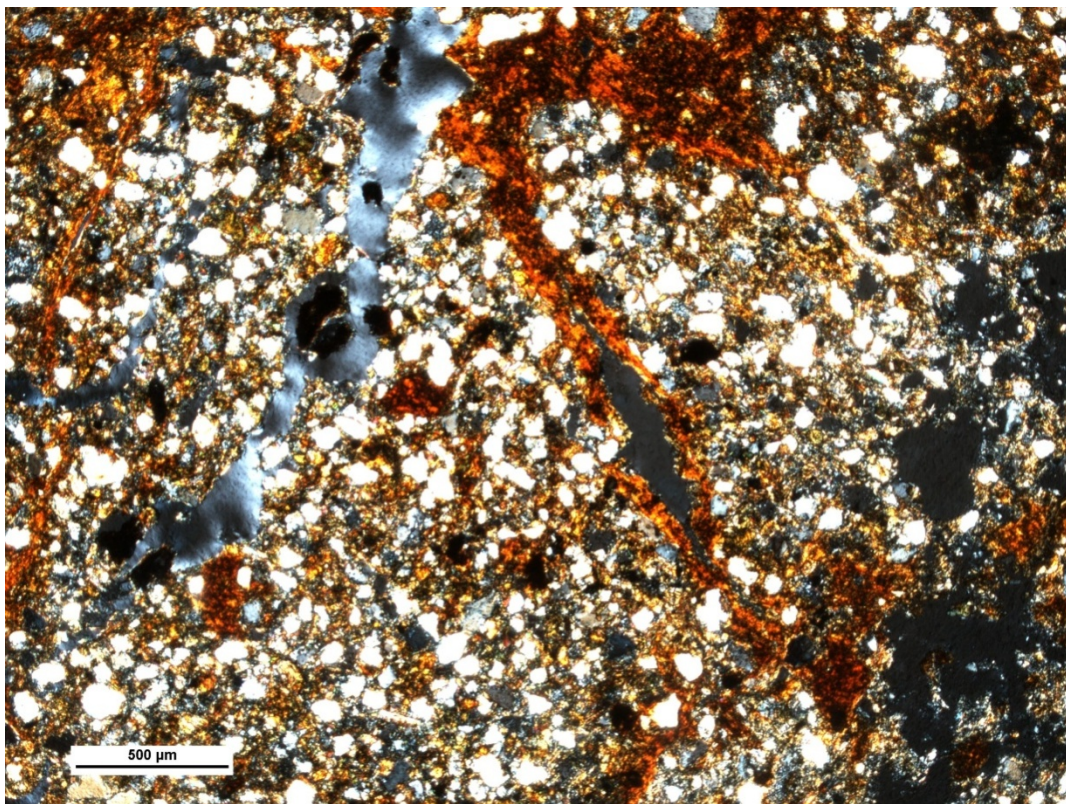
Figure 23: Transmitted cross-polarised light micrograph from the C horizon of the Keyneton profile.
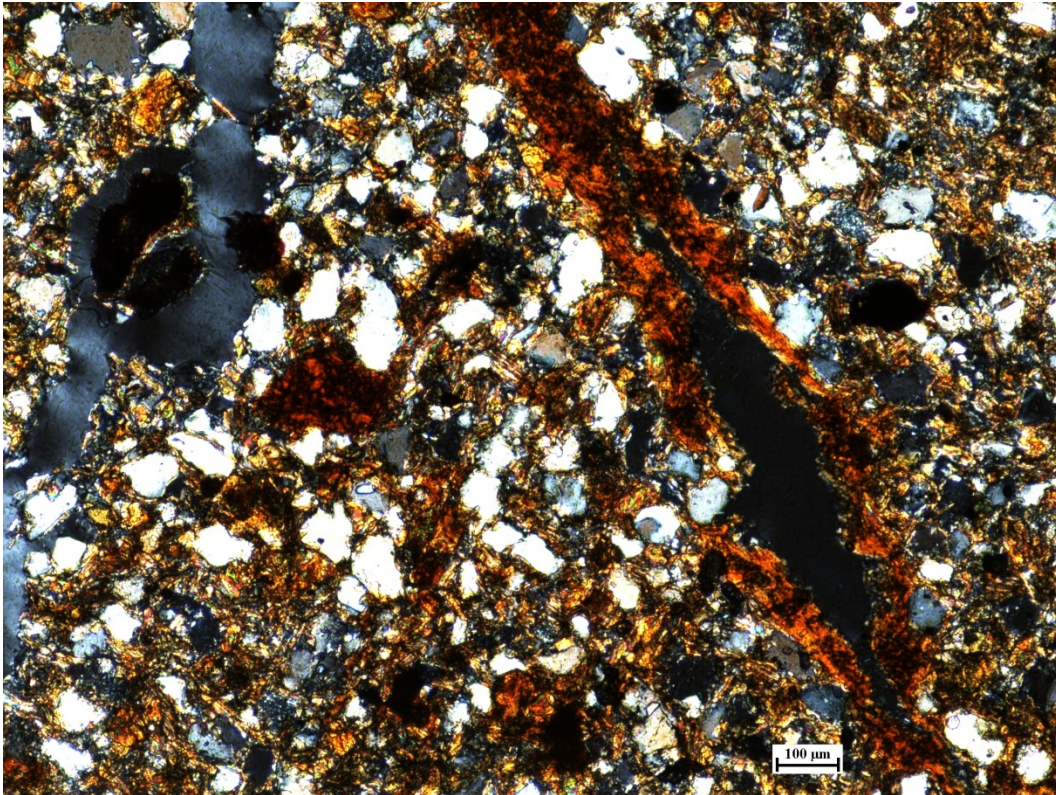
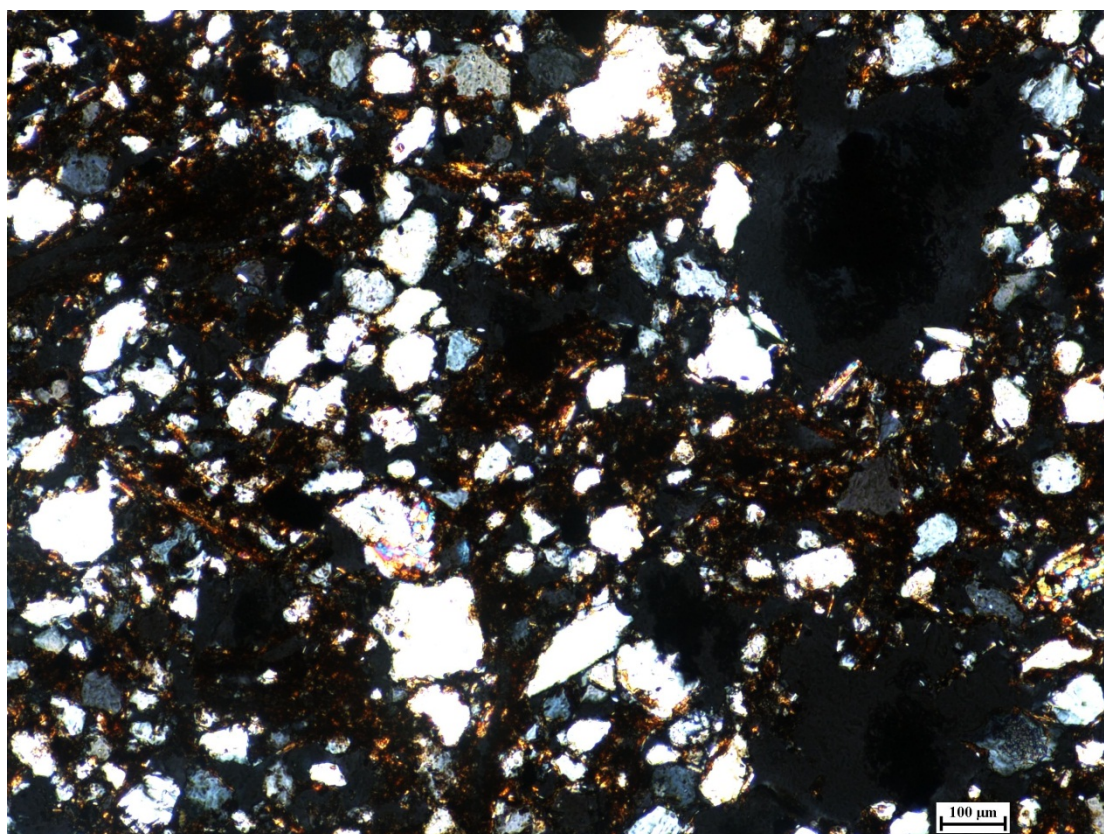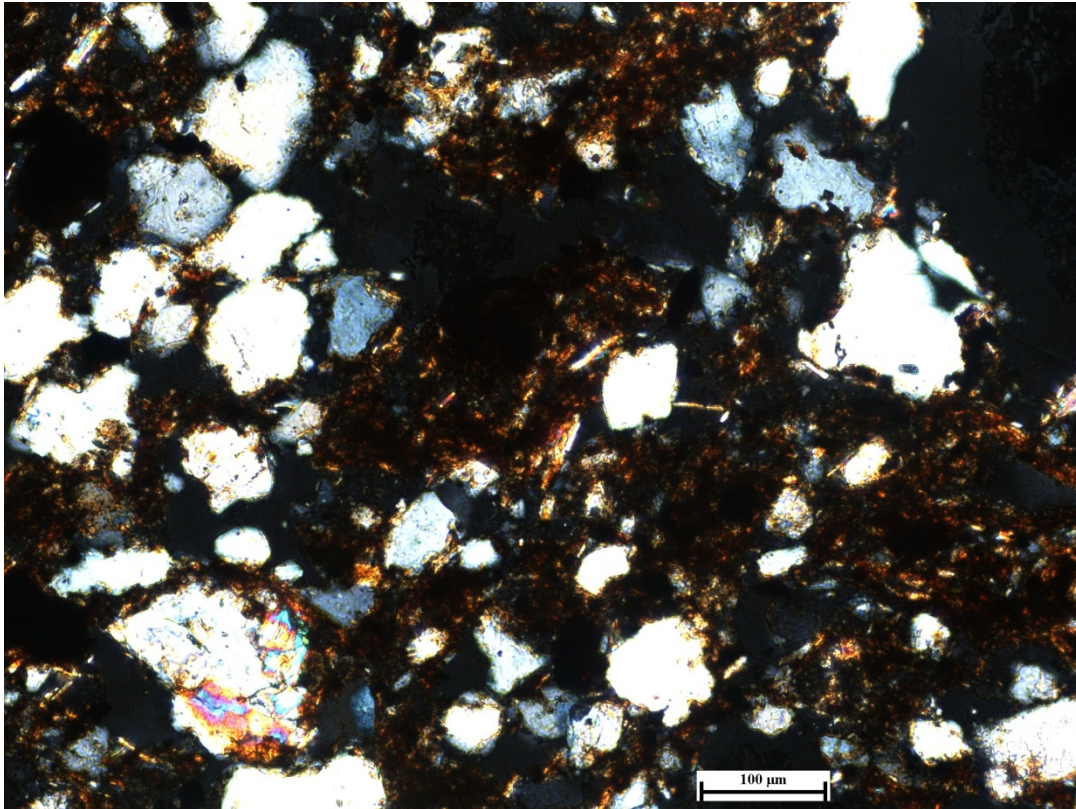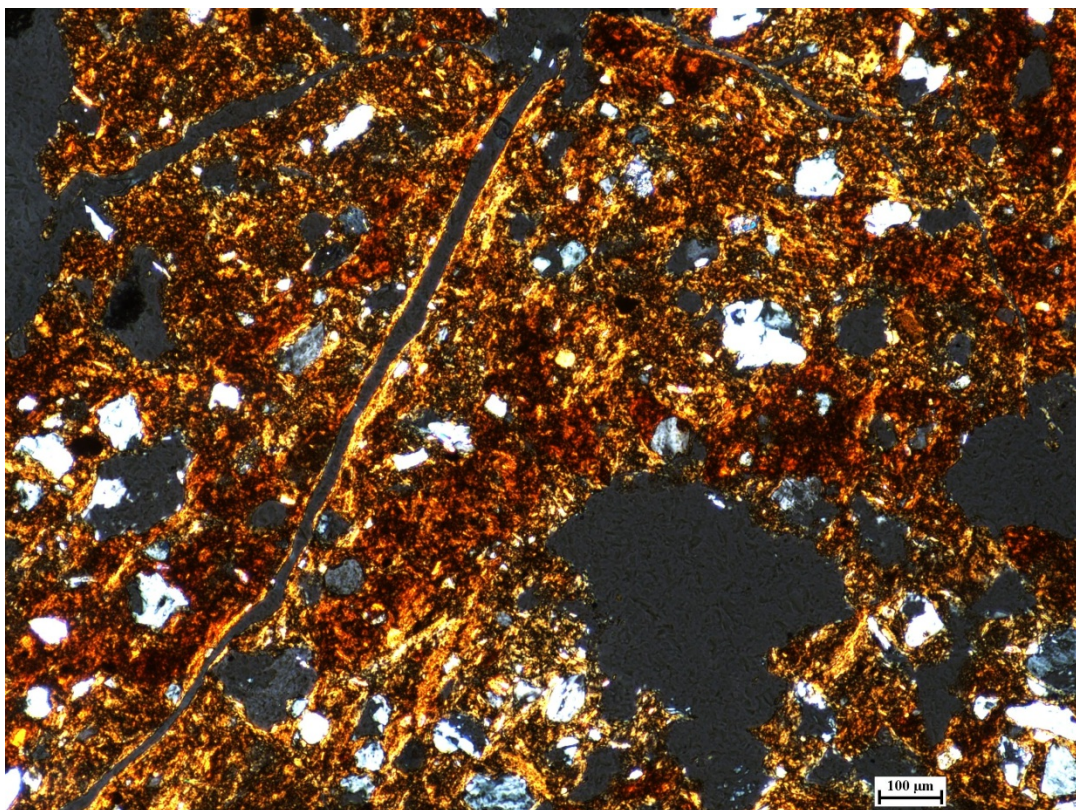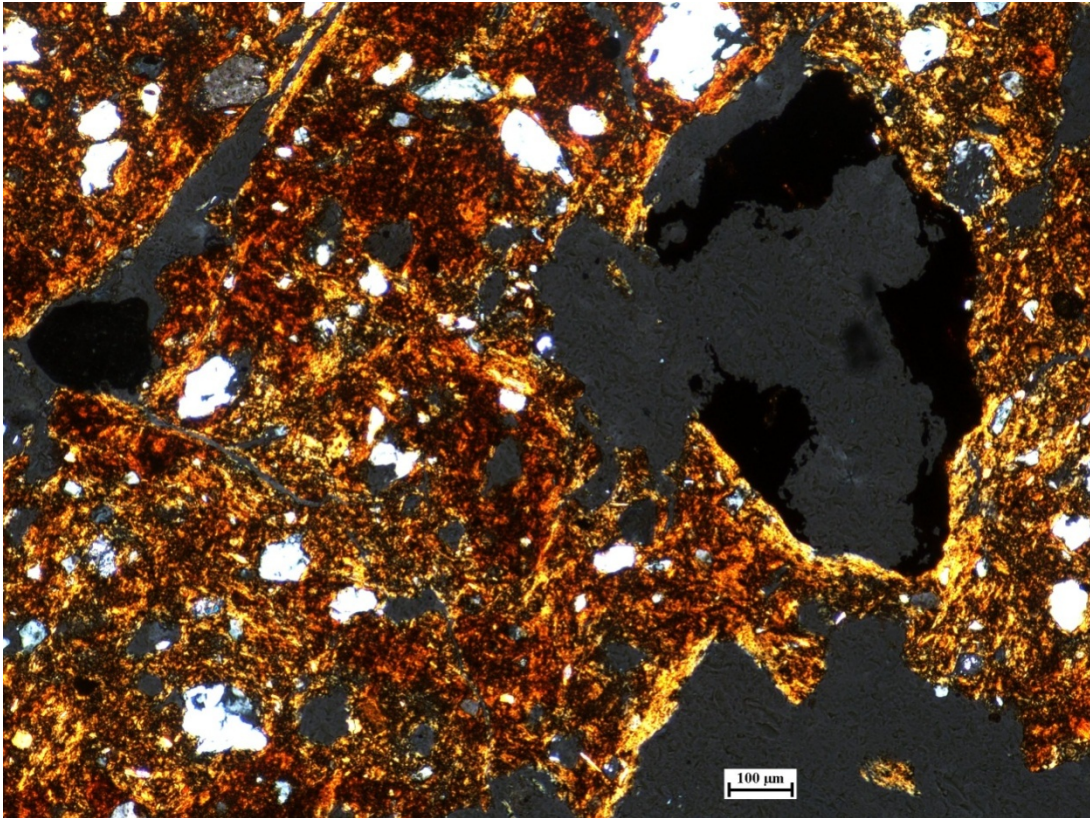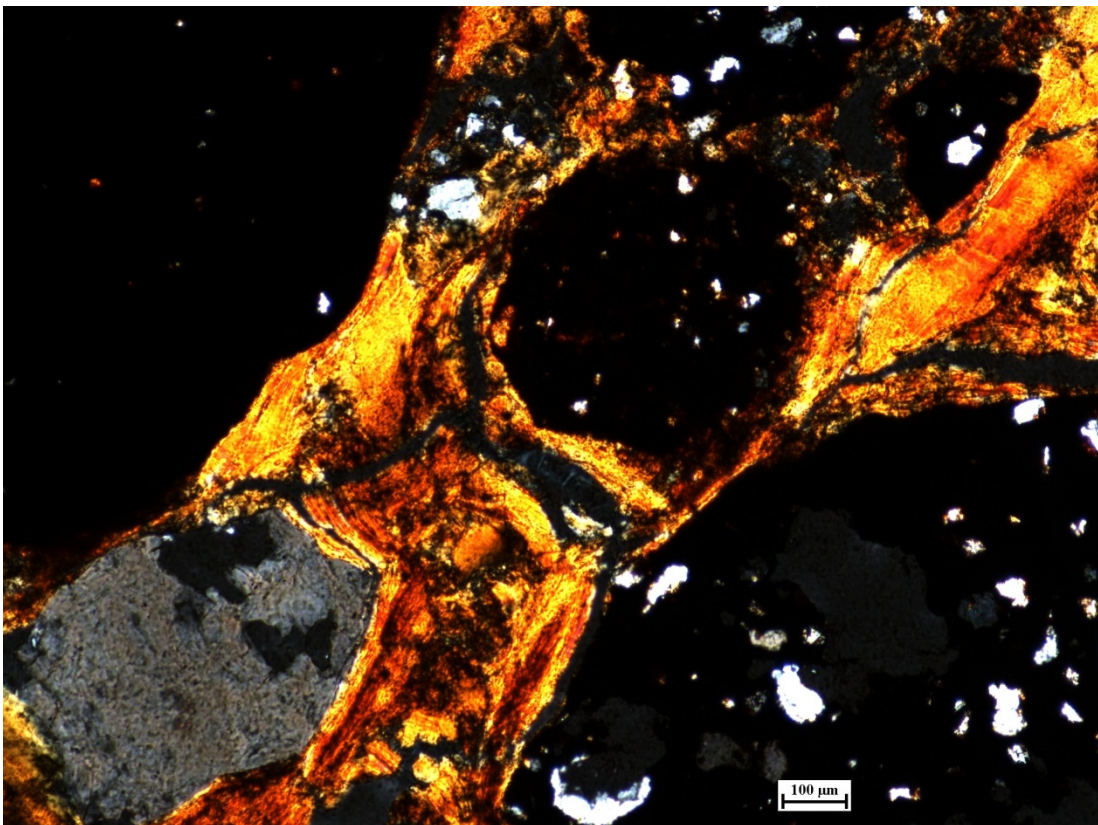**Figure 24: Transmitted cross-polarised light micrograph from the C horizon of the Keyneton profile.**

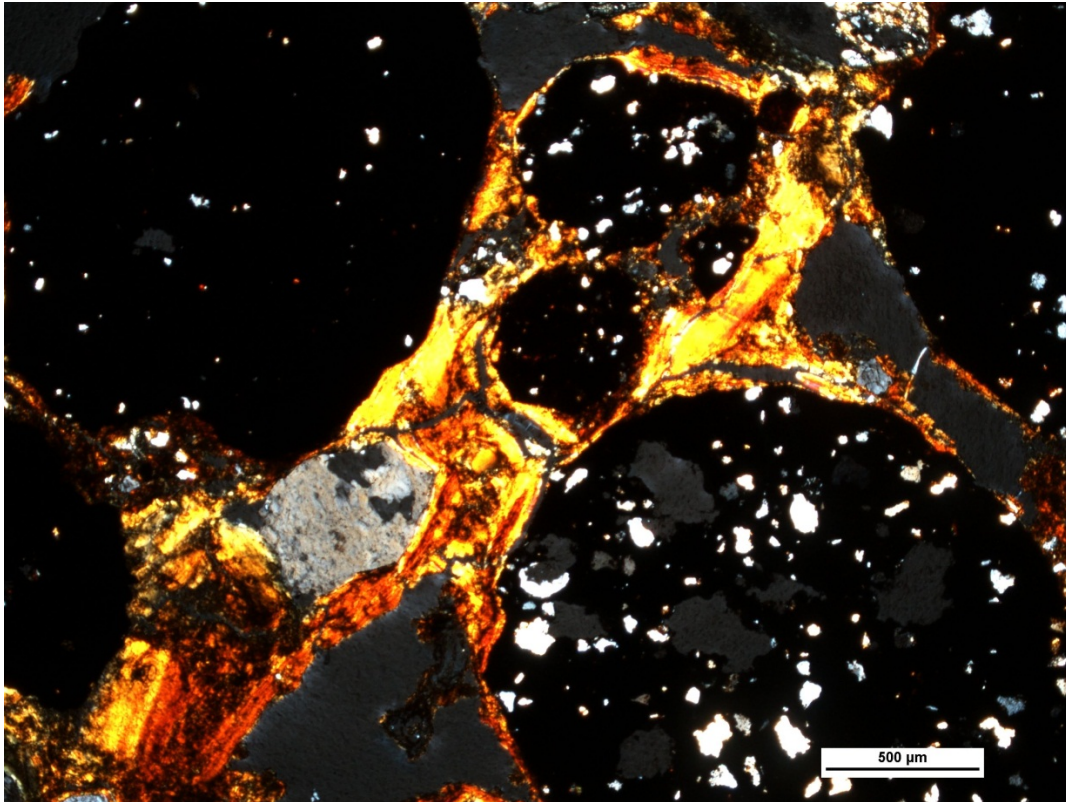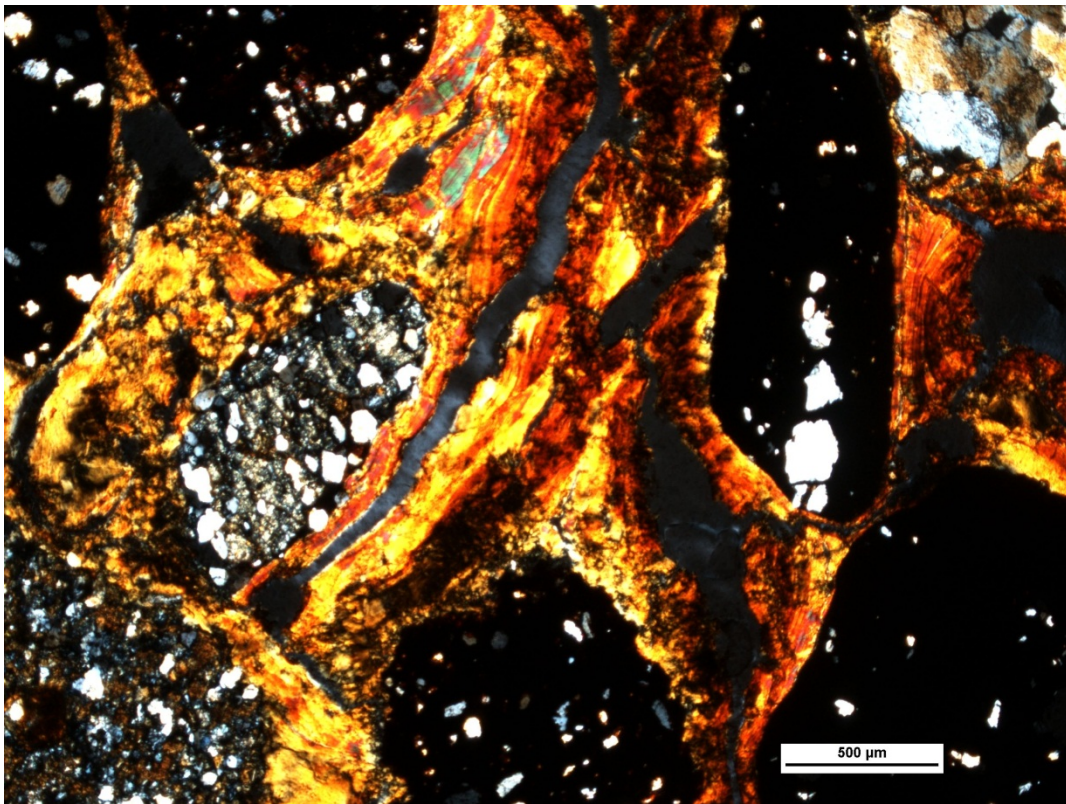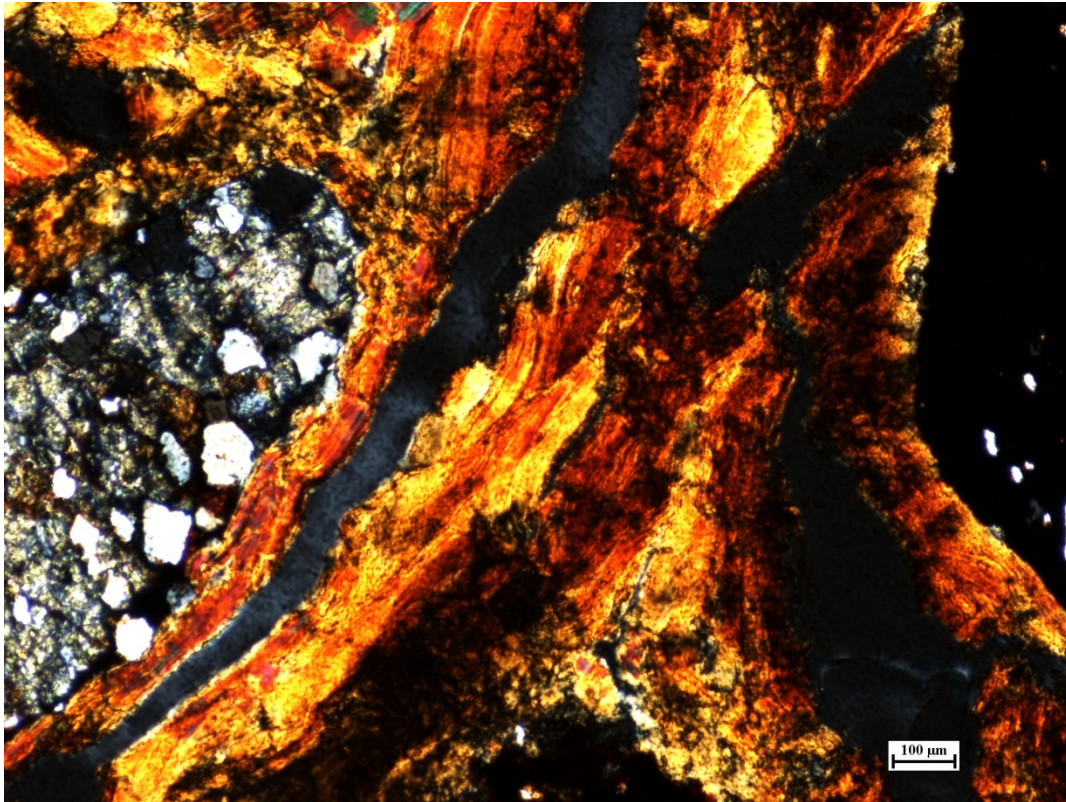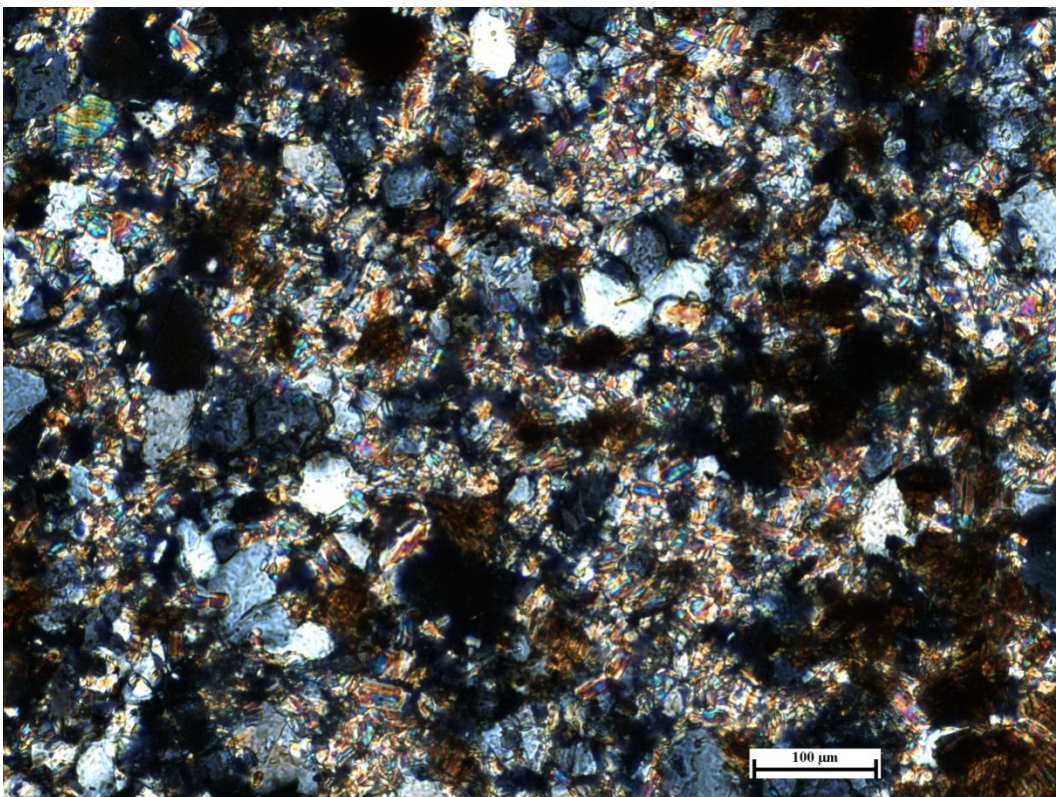**Figure 25: Transmitted cross-polarised light micrograph from the R horizon of the Keyneton profile.**

APPENDIX D: CHEMICAL ANALYSIS

Sample preparation

Soil from the bulk samples of each Keyneton profile horizon, ~10 g, was ground to a fine powder using a tungsten carbide mill at the University of Adelaide's Waite campus.

In addition to the whole soil samples, samples from the 20-63μm and 63-125μm fractions of the Keyneton profile were prepared. Samples of ~5 g from each horizon and size fraction were taken during sieving analysis and oven dried. The size fraction samples did not include the parent material.

Analysis

Samples were taken to Intertek Genalysis (Adelaide Facility) for determination of chemical copmpsition. Major elements were analysed for by inductively coupled plasma optical emission spectroscopy (ICP-OES) and minor/trace elements by inductively coupled plasma mass spectrometry (ICP-MS). Lithium borate fusion digest was used for all samples.

Table 14: Element and oxide concentrations from the Keyneton profile.

Horizon	Size fraction	Al (wt. %)	Al_2O_3 (wt. %)	Ca (wt. %)	CaO (wt. %)	Ce (ppm)	Fe (wt. %)	Fe_2O3 (wt. %)	K (wt. %)	K_2O (wt. %)
A1	whole soil	5.19	9.8	0.34	0.47	67.7	3.52	5.03	1.06	1.27
A2	whole soil	3.62	6.85	0.16	0.23	53.9	10.12	14.47	0.72	0.87
B21	whole soil	8.62	16.3	0.15	0.21	95.4	9.22	13.18	1	1.2
B22	whole soil	8.06	15.24	0.13	0.18	136.6	10.39	14.85	0.99	1.19
C	whole soil	7.99	15.1	0.41	0.57	355.4	4.62	6.6	1.72	2.07
R	whole soil	7.32	13.83	0.03	0.05	65.6	3.4	4.86	2.74	3.3
A1	63-125 μm	2.04	3.85	0.25	0.34	27.2	1.12	1.6	0.45	0.54
A2	63-125 μm	1.51	2.86	0.16	0.22	15.6	0.71	1.01	0.37	0.44
B21	63-125 μm	1.24	2.34	0.11	0.15	16.5	0.55	0.78	0.31	0.38
B22	63-125 μm	1.56	2.94	0.09	0.12	38.1	1.28	1.83	0.39	0.47
C	63-125 μm	2.27	4.29	0.06	0.08	44.3	1.59	2.27	1	1.21
A1	20-63 μm	3.42	6.46	0.31	0.44	51.1	1.83	2.61	1.01	1.22
A2	20-63 μm	2.8	5.29	0.21	0.29	68.4	1.48	2.12	0.81	0.98
B21	20-63 μm	2.7	5.09	0.18	0.26	76.8	1.19	1.7	0.81	0.97
B22	20-63 μm	3.04	5.75	0.18	0.25	91.6	2.25	3.22	1.06	1.28
C	20-63 μm	4.89	9.25	0.1	0.14	81.5	4.75	6.79	2.66	3.21

Table 15: Element and oxide concentrations from the Keyneton profile. 'X' indicates a concentration below the detection limit of the instrument.

Horizon	Size fraction	Mg (wt. %)	MgO (wt. %)	Mn (wt. %)	MnO (wt. %)	Na (wt. %)	Na$_2$O (wt. %)	Nb (ppm)	Nd (ppm)
A1	whole soil	0.38	0.64	0.02	0.03	0.39	0.53	11.2	30.8
A2	whole soil	0.19	0.32	0.02	0.03	0.34	0.46	9.4	23.2
B21	whole soil	0.5	0.83	0.01	X	0.25	0.33	12.3	51.7
B22	whole soil	0.53	0.88	0.02	0.03	0.22	0.3	9.5	72.4
C	whole soil	1.14	1.88	0.04	0.05	0.14	0.19	18	200.1
R	whole soil	0.8	1.33	0.04	0.05	0.13	0.17	22.2	38.8
A1	63-125 μm	0.13	0.22	X	X	0.43	0.58	X	11.8
A2	63-125 μm	0.1	0.16	X	X	0.45	0.6	X	6.8
B21	63-125 μm	0.08	0.13	X	X	0.33	0.44	X	7.5
B22	63-125 μm	0.08	0.13	0.01	X	0.37	0.5	X	14.8
C	63-125 μm	0.4	0.66	0.01	X	0.07	0.1	6.8	27.8
A1	20-63 μm	0.22	0.37	0.02	0.03	0.9	1.21	8.2	22.3
A2	20-63 μm	0.13	0.21	0.02	0.03	0.73	0.98	11.6	29.1
B21	20-63 μm	0.1	0.17	0.02	0.03	0.72	0.97	11.6	33.4
B22	20-63 μm	0.19	0.32	0.02	0.03	0.68	0.92	13.4	35
C	20-63 μm	1.28	2.13	0.07	0.09	0.12	0.17	39.8	55.5

Table 16: Element and oxide concentrations from the Keyneton profile. 'X' indicates a concentration below the detection limit of the instrument.

Horizon	Size fraction	P (wt. %)	P_2O_5 (wt. %)	Si (wt. %)	SiO_2 (wt. %)	Th (ppm)	Ti (wt. %)	TiO_2 (wt. %)	Y (ppm)	Zr (ppm)
A1	whole soil	0.04	0.08	30.87	66.05	13.12	0.3	0.5	27	382
A2	whole soil	0.02	0.04	33.18	70.98	20.5	0.28	0.47	24.8	454
B21	whole soil	0.01	0.03	26.64	56.99	28.32	0.4	0.67	38	338
B22	whole soil	0.01	0.03	26.86	57.46	27.49	0.37	0.62	53.5	356
C	whole soil	0.03	0.07	29.43	62.96	39.88	0.54	0.9	197.5	868
R	whole soil	X	X	32.65	69.85	32.06	0.61	1.02	53.5	939
A1	63-125 µm	0.03	0.06	38.9	83.21	5.18	0.12	0.2	12.1	225
A2	63-125 µm	X	X	44.06	94.27	3.09	0.11	0.18	11.6	298
B21	63-125 µm	X	X	44.86	95.97	2.78	0.09	0.16	9.5	180
B22	63-125 µm	X	X	43.66	93.39	4.97	0.14	0.23	14.9	401
C	63-125 µm	0.01	0.03	42.24	90.35	9.63	0.27	0.45	25	315
A1	20-63 µm	0.02	0.05	37.31	79.83	10.87	0.35	0.58	29.7	652
A2	20-63 µm	0.02	0.05	40.79	87.27	13.51	0.46	0.76	46	1324
B21	20-63 µm	0.03	0.06	41.63	89.06	13.03	0.43	0.72	47.2	1425
B22	20-63 µm	0.02	0.05	40.13	85.85	14.05	0.47	0.79	51.8	1635
C	20-63 µm	X	X	33.71	72.11	26.75	1.23	2.05	106	4091

APPENDIX E: ASSESSING UNIFORMITY OF THE PARENT MATERIAL

Elemental ratios

Ratios of concentrations of elements known to be found in minerals resistant to weathering were calculated with depth for the Keyneton profile.

Table 17: Elemental ratios from the 20-125 μm fraction of the Keyneton profile

Horizon	$Zr_{20-125\mu m}/Ti_{20-125\mu m}$	$Nd_{20-125\mu m}/Zr_{20-125\mu m}$	$Y_{20-125\mu m}/Zr_{20-125\mu m}$
A1	0.187	0.039	0.048
A2	0.285	0.022	0.036
B21	0.309	0.025	0.035
B22	0.334	0.024	0.033
C	0.294	0.019	0.030

Table 18: Elemental ratio from the whole soil (i.e. all particle sizes) fraction of the Keyneton profile.

Horizon	$Nb_{whole\ soil}/Zr_{whole\ soil}$
A1	0.029
A2	0.021
B21	0.036
B22	0.027
C	0.021
R	0.024

APPENDIX F: EXTENT OF WEATHERING

Weathering indices

To quantify the degree of weathering throughout the Keyneton profile, two weathering indices were applied:

The chemical index of alteration (CIA) developed by Nesbitt & Young (1982):

$$CIA = [Al_2O_3/(Al_2O_3 + CaO + Na_2O + K_2O)]*100$$

The chemical index of weathering (CIW) developed by Harnois (1988):

$$CIW = [Al_2O_3/(Al_2O_3 + CaO + Na_2O)]*100$$

In calculating these indices, molecular proportions of the oxides were used.

Table 19: Weathering indices for each horizon of the Keyneton profile.

Horizon	CIA	CIW
A1	75.96	85.02
A2	76.39	85.36
B21	88.00	94.63
B22	87.84	94.89
C	80.79	91.80
R	77.82	97.39

APPENDIX G: BULK DENSITY

Intact clod method

Bulk density measurements of each horizon from the Keyneton soil profile were obtained with use of the clod method outlined by Grossman & Reinsch (2002). Given the high gravel content of some samples, the correction for coarse fragments provided by Carter (2003) was incorporated.

The A1 horizon of the Keyneton profile had very weak structure; therefore, no clod samples or measurements were obtained for that horizon.

Apparatus:
Top-weighing laboratory balance
Wax bath
Retort stand & clamp
Cotton thread
Beaker (1L)
Thermometer
Oven

Materials:
Intact clods (three from each soil horizon)
Paraffin wax
Water

Procedure:
1. The wax bath was heated to a temperature just above the melting point of paraffin wax (~60°C).
2. A small subsample of the clod (~15 g) was taken and the weight recorded (W_4). The subsample was oven-dried and re-weighed (W_5).
3. Cotton thread was attached around the clod to form a cradle and the weight of this sample was recorded (W_1).
4. The clod was dipped quickly into the paraffin wax bath once and withdrawn to avoid wax penetration. The wax coating was examined and, if required, the clod was again dipped into the wax to ensure an entirely sealed coating.
5. The wax-coated clod was cooled to room temperature and weighed (W_2).
6. A 1L beaker filled with enough water to allow total clod immersion was placed onto the top-weighing balance. The balance was then re-zeroed.
7. The wax-coated clod was suspended from the retort stand and totally immersed in the water. The weight of the wax-coated clod in water was recorded (W_3).
8. The above procedure was followed for three intact clods from each horizon (excluding the A1 horizon due to the soil being too loose to obtain intact clods), resulting in a total of 15 clods.

Calculations:
Density of wax (ρ_{wax}): $\qquad\qquad\qquad\qquad$ $\rho_{wax}= 0.92$ Mg.m^{-3}

Density of water (ρ_{water}): $\rho_{water} = 1.00$ Mg.m^{-3}

Weight of wax (W_{wax}): $W_{wax} = W_2 - W_1$

Volume of wax (V_{wax}): $V_{wax} = W_{wax}/\rho_{wax}$

Water content of clod (θ_g): $\theta_g = (W_4 - W_5)/W_5$

Dry weight of original clod (M_s): $M_s = W_1/(1 + \theta_g)$

Volume of original clod (V_{clod}): $V_{clod} = (W_3/\rho_{water}) - V_{wax}$

Bulk density of original clod (ρ_b): $\rho_b = M_s/V_{clod}$

Table 20: Bulk density measurements, corrected for coarse fragments, for three intact clod samples from each horizon of the Keyneton profile.

Horizon	Sample	Bulk density, ρ_b (g/cm^3)
A2	a	1.29
A2	b	1.24
A2	c	1.25
B21	a	1.51
B21	b	1.70
B21	c	1.69
B22	a	1.77
B22	b	1.87
B22	c	1.52
C	a	1.38
C	b	1.35
C	c	1.57
R	a	2.05
R	b	1.95
R	c	1.98

Table 21: Average bulk density for each horizon from the Keyneton profile.

Horizon	Average bulk density, ρ_b (g/cm^3)
A2	1.26
B21	1.63
B22	1.72
C	1.43
R	1.99

APPENDIX H: THE MASS BALANCE MODEL

The derivation of the equations used for the calculation volume and chemical constituent fluxes from the Keyneton profile is provided by Brimhall *et al.* (1987, 1988 1991, 1992) and Chadwick *et al.* (1990). The calculation for mass gain/loss has largely been derived from Brewer (1976).

Strain

Strain ($\varepsilon_{i,w}$) represents the volume change in a soil profile and is calculated with respect to an immobile index element.

$$\varepsilon_{i,w} = [\, (\rho_p C_{i,p})/(\rho_w C_{i,w})] - 1$$

Where: ρ_p is the bulk density of the parent material, ρ_w is the bulk density of the weathered soil horizon, $C_{i,p}$ is the concentration of the immobile index element in the parent material, and $C_{i,w}$ is the concentration of the immobile index element in the weathered soil horizon (Chadwick *et al.* 1990).

The value for strain is has no units; however, it represents the percentage of volume gain or loss from a soil profile (e.g. a strain value of +1.3 represents a 130% increase in volume resulting from soil formation).

Transported mass fraction

The transported mass fraction ($\tau_{j,w}$), or open-system mass transport function, is used to quantify the gains of chemical constituents from a soil profile (Brimhall *et al.* 1988; Chadwick *et al.* 1990).

$$\tau_{j,w} = [(\rho_w C_{j,w})/(\rho_p C_{j,p})] \times (\varepsilon_{i,w}+1) - 1$$

Where: ρ_w is the bulk density of the weathered soil horizon, $C_{j,w}$ is the concentration of the element under investigation in the weathered soil horizon, ρ_p is the bulk density of the parent material, $C_{j,p}$ is the concentration of the element under investigation in the parent material, and $\varepsilon_{i,w}$ is the strain of the weathered soil horizon with respect to the immobile index element (Chadwick *et al.* 1990).

The transported mass fraction $\tau_{j,w}$ has no units, as it represents the percentage loss of the mass of element j.

Mass gain or loss

The equation used to calculate the mass gained or lost during soil formation has been derived from Brewer (1976). It allows the quantification of mass flux from a volume of soil profile equal to 1cm^2 multiplied by the depth of the horizon or profile of interest.

The mass of the present day soil horizon (m_w), in grams, is given by:

$$m_w = \rho_w \times V_w$$

Where ρ_w is the bulk density of the soil horizon (g/cm^3), and V_w is the volume of the present day soil horizon given by:

$$V_w = d \times 1cm^2$$

Where d is the depth (height) of the present day soil horizon, in cm.

From the mass of the present day soil horizon (m_w) it is possible to determine the mass of the parent material (m_p) from which it originated, with respect to an immobile index element.

$$m_p = (C_{i,w}/C_{i,p}) \times m_w$$

Where $C_{i,w}$ is the concentration of the immobile index element in the weathered soil horizon, and $C_{i,p}$ is the concentration of the immobile index element in the parent material.

The change in mass (Δm) is then given by the difference between the mass of the parent material (m_p) and the mass of the present day soil horizon (m_w).

$$\Delta m = m_p - m_w$$

APPENDIX I: X-RAY DIFFRACTION ANALYSIS

Subsamples of the clay suspensions attained during particle size distribution work were taken to CSIRO Land & Water for x-ray diffraction analysis:

The CSIRO used the following method:

XRD patterns were recorded with a PANalytical X'Pert Pro Multi-purpose Diffractometer using an automatic divergence slit, 2° anti-scatter slit and fast X'Celerator Si strip detector. XRD data was collected with Fe-filtered CoKα radiation. The diffraction patterns were recorded in steps of 0.017° 2θ with a 2.0 second counting time per step, and logged to data files for analysis.